KCL-PH-TH/2016-20, LCTS/2016-13, CERN-PH-TH/2016-095
UMN-TH-3526/16, FTPI-MINN-16/16

arXiv:1605.01398v2 [hep-ph] 3 Oct 2016

Maximal Sfermion Flavor Violation in Super-GUTs

John Ellis[1], **Keith A. Olive**[2] and **L. Velasco-Sevilla**[3]

[1] *Theoretical Particle Physics and Cosmology Group, Department of Physics, King's College London, London WC2R 2LS, United Kingdom; Theoretical Physics Department, CERN, CH-1211 Geneva 23, Switzerland*

[2] *William I. Fine Theoretical Physics Institute, School of Physics and Astronomy, University of Minnesota, Minneapolis, MN 55455, USA*

[3] *University of Bergen, Department of Physics and Technology, PO Box 7803, 5020 Bergen, Norway*

Abstract

We consider supersymmetric grand unified theories with soft supersymmetry-breaking scalar masses m_0 specified above the GUT scale (super-GUTs) and patterns of Yukawa couplings motivated by upper limits on flavour-changing interactions beyond the Standard Model. If the scalar masses are smaller than the gaugino masses $m_{1/2}$, as is expected in no-scale models, the dominant effects of renormalization between the input scale and the GUT scale are generally expected to be those due to the gauge couplings, which are proportional to $m_{1/2}$ and generation-independent. In this case, the input scalar masses m_0 may violate flavour maximally, a scenario we call MaxSFV, and there is no supersymmetric flavour problem. We illustrate this possibility within various specific super-GUT scenarios that are deformations of no-scale gravity.

October 2016

1 Introduction

Ever since the earliest days of supersymmetric model-building, it has been emphasized that data on flavour-changing processes suggest the existence of a 'super-GIM' mechanism to ensure that the effective electroweak-scale slepton and squark mass matrices are almost diagonal with small generational mixing and eigenvalues that are almost degenerate [1]. This constraint on supersymmetric model-building has subsequently been dubbed the 'supersymmetric flavour problem'. Soon after [1], it was recognized that one possible scenario for solving this 'problem' in the squark sector would be to postulate that all supersymmetric flavour violation is proportional to the Cabibbo-Kobayashi-Maskawa (CKM) mixing between quarks [2], a scenario that has come to be known as minimal flavour violation (MFV). This approach left open the question how MFV came to be, one possible answer being provided by gaugino mediation of supersymmetry breaking [3].

A suitable framework for studying the supersymmetric flavour problem is provided by a supersymmetric GUT such as SU(5) [4, 5] in which the soft supersymmetry-breaking scalar masses m_0, the trilinear soft supersymmetry-breaking parameters A_0 and the gaugino masses $m_{1/2}$ are input at the GUT scale $M_{GUT} \simeq 10^{16}$ GeV. Upper limits on the deviations from Standard Model predictions for flavour-changing processes motivate the hypothesis that the m_0 parameters for chiral supermultiplets with the same gauge quantum numbers are identical at this input scale [2], and the GUT symmetry requires them to be identical for all the sparticles in the same GUT multiplet. Thus, in SU(5) all the $\bar{\mathbf{5}}$ sfermions would have a common m_0, and all the **10** sfermions would have another (potentially different) common m_0. It is often assumed, with no clear phenomenological motivation apart from simplicity and possible embedding in a larger supersymmetric GUT such as SO(10), that these two m_0 parameters are identical at the GUT scale, a scenario called the constrained minimal supersymmetric extension of the standard model or CMSSM [6].

The question remains, however, what might be the origin of any such universality in the m_0 parameters. This would occur in minimal supergravity models with trivial, flat Kähler metrics [7], but would not happen in more general supergravity models [8], as discussed recently in the context of compactified M-theory [9]. One interesting exception is no-scale supergravity [11], in which the input soft supersymmetry-breaking scalar masses m_0 vanish at the input scale. In this case, the electroweak-scale soft supersymmetry-breaking scalar masses are all generated by gauge interactions, and hence are identical for different sparticles with the same gauge quantum numbers, in a manner reminiscent of gauge-mediated supersymmetry-breaking models [12]. The phenomenological constraints on sparticle masses exclude models with no-scale boundary conditions at the supersymmetric GUT scale [13], but no-scale boundary conditions at higher input scales may be acceptable [13, 14, 15].

The principal purpose of this paper is to study the constraints on the flavour structure of the soft supersymmetry-breaking scalar masses for models that are similar to such no-scale models, with $m_0 \ll m_{1/2}$ at some input scale $M_{in} > M_{GUT}$, scenarios we call super-GUTs. One may regard such scenarios as deformations of the simple no-scale framework, as might occur in realistic string models via higher-order corrections to the (over-simplistic?) no-scale Kähler potential, cf, the studies in [9]. Intuitively, it is clear that the constraints on the non-universalities between the diagonal m_0 parameters and on the ratios of off-diagonal to diagonal entries in the soft supersymmetry-breaking scalar mass matrix must become progressively weaker as the no-scale limit: $m_0 \to 0$ is approached.

Indeed, close to this no-scale limit a completely anarchic m_0 matrix is allowed. In this sense, we consider possible anarchic structures which we term as maximal flavour violation

(MaxSFV). Thus, there is no 'supersymmetric flavour problem' for super-GUTs with input boundary conditions at some scale $M_{in} > M_{GUT}$ that are small deformations of the idealised no-scale limit. A primary objective of this paper is to quantify this statement within illustrative super-GUT scenarios.

The effects of flavor-violating sfermion mass parameters on hadronic and leptonic flavor observables, as well as their correlations, have been studied previously in the context of Grand Unified Theories. These studies typically assume the mass insertion approximation without a complete top-down running of the soft supersymmetry-breaking parameters (see, e.g., [10]). We do not strive to study the generalities of such correlations, instead we consider a specific set up where we establish limits on the maximal values of the off-diagonal entries in the m_0 matrix using a complete running of soft supersymmetry-breaking parameters. Also, we constrain the parameter space via EW observables as well as flavor-violating effects. To our knowledge, this is the first complete and realistic study that takes into account running from a scale above the unification scale.

The layout of this paper is as follows. We begin in Section 2 by setting up our super-GUT model framework [13, 16, 17, 14, 18], focusing in particular on its implementation in no-scale supergravity [14]. We use weak-scale measurements to specify the gauge and Yukawa couplings, whereas the soft supersymmetry-breaking scalar masses, trilinear and bilinear terms are specified at the input scale, M_{in}. The matching conditions at M_{GUT} are discussed in Section 2.3. We then specify in Section 2.4 the illustrative flavour-mixing models that we choose for further study. In Section 3 we analyse the case of pure no-scale boundary conditions, in which all soft supersymmetry-breaking scalar masses, trilinear and bilinear terms are set to zero at M_{in}. We display the running of of these parameters as well as the Yukawa couplings between the input and weak scales for our representative flavour-mixing scenarios. Then, in Section 4 we analyse super-GUT scenarios in which $M_{in} > M_{GUT}$, studying the upper bounds on non-universality in $m_0/m_{1/2}$ that are permitted by the experimental upper limits on flavour-changing interactions as functions of M_{in} in our illustrative flavour-mixing scenarios. Finally, Section 5 summarises our conclusions.

2 Model Framework

2.1 No-scale SUGRA model

We first consider a low-energy effective theory that is based on an $N = 1$ supergravity model with the simplest no-scale structure [11] defined by a Kähler potential

$$K \;=\; -3\ln(T + T^\dagger - \sum_i |\Phi_i|^2/3) \tag{1}$$

where T is a modulus field and Φ represents matter fields present in the theory. The no-scale form (1) for K ensures that all soft supersymmetry-breaking scalar masses and bi- and trilinear terms vanish at some input universality scale, M_{in}. However, we recall that non-zero gaugino masses arise independently from a non-trivial gauge kinetic function $f_{\alpha\beta}$ in the effective supergravity theory. It is known that vanishing soft masses at the GUT scale M_{GUT} in a theory with universal gaugino masses are in general phenomenologically disastrous [13]. However, this problem may be circumvented if the input universality scale is between the GUT scale and the Planck scale [13, 14, 15].

A Kähler potential of the form (1) arises in generic manifold compactifications of string theory, in which T is identified as the manifold volume modulus. In such a scenario, the

Φ_i are identified as untwisted matter fields. In general there would, in addition, be twisted matter fields φ_a described by additional terms in the Kähler potential of the form

$$\Delta K \; = \; \sum_a \frac{|\varphi_a|^2}{(T+T^\dagger)^{n_a}} \,, \tag{2}$$

where the parameters n_a are model-dependent modular weights. These give rise to n_a-dependent soft supersymmetry-breaking terms whose magnitudes and flavour structure are also model-dependent and violate the MFV assumption, in general. Here, we assume that the MSSM matter fields are assigned to the untwisted sector.

The renormalization of MSSM parameters at scales above M_{GUT} requires the inclusion of new particles and parameters in addition to those in the generic MSSM, including GUT-scale Higgses, their self-couplings and couplings to matter. For simplicity, we assume here minimal SU(5), in which one introduces a single SU(5) adjoint Higgs multiplet $\hat{\Sigma}(\mathbf{24})$, and the two Higgs doublets of the MSSM, $\hat{H}_d$ and $\hat{H}_u$, are extended to five-dimensional SU(5) representations $\hat{\mathcal{H}}_1(\overline{\mathbf{5}})$ and $\hat{\mathcal{H}}_2(\mathbf{5})$ respectively. The minimal renormalizable superpotential for this model is [19, 17]

$$\begin{aligned} W_5 \;\; = \;\; & \mu_\Sigma \, \mathrm{Tr}\, \hat{\Sigma}^2 + \frac{1}{6}\lambda' \, \mathrm{Tr}\, \hat{\Sigma}^3 + \mu_H \hat{\mathcal{H}}_{1\alpha} \hat{\mathcal{H}}_2^\alpha + \lambda \hat{\mathcal{H}}_{1\alpha} \hat{\Sigma}^\alpha_\beta \hat{\mathcal{H}}_2^\beta \\ & + \frac{1}{4} (\mathbf{h_{10}})_{ij} \epsilon_{\alpha\beta\gamma\delta\zeta} \hat{\psi}_i^{\alpha\beta} \hat{\psi}_j^{\gamma\delta} \hat{\mathcal{H}}_2^\zeta + \sqrt{2} (\mathbf{h_{\overline{5}}})_{ij} \hat{\psi}_i^{\alpha\beta} \hat{\phi}_{j\alpha} \hat{\mathcal{H}}_{1\beta}, \end{aligned} \tag{3}$$

where Greek letters denote SU(5) indices, $i, j = 1..3$ are generation indices and ϵ is the totally antisymmetric tensor with $\epsilon_{12345} = 1$. The $\hat{D}_i^c$ and $\hat{L}_i$ superfields of the MSSM reside in the $\overline{\mathbf{5}}$ representations, $\hat{\phi}_i$, while the $\hat{Q}_i$, $\hat{U}_i^c$ and $\hat{E}_i^c$ superfields are in the $\mathbf{10}$ representations, $\hat{\psi}_i$. The new dimensional parameters μ_H and μ_Σ are of $\mathcal{O}(M_{GUT})$. The soft supersymmetry breaking part of the Lagrangian involving scalar components of chiral superfields can then be written as

$$\begin{aligned} \mathcal{L}_{soft}(\psi, \phi) \;\; \ni \;\; & -m_{\bar{5}}^2 |\phi|^2 - m_{10}^2 \mathrm{Tr}\left[\psi^\dagger \psi\right] \\ & + \left[b_\Sigma \, \mathrm{Tr}\, \hat{\Sigma}^2 + \frac{1}{6} a' \, \mathrm{Tr}\, \hat{\Sigma}^3 + b_H \hat{\mathcal{H}}_{1\alpha} \hat{\mathcal{H}}_2^\alpha + a \hat{\mathcal{H}}_{1\alpha} \hat{\Sigma}^\alpha_\beta \hat{\mathcal{H}}_2^\beta \right] \\ & + \left[\frac{1}{4} \, a_{10} \, \epsilon_{ijklm} \psi^{ij} \psi^{kl} \, \hat{\mathcal{H}}_2^m + \sqrt{2} \, a_{\bar{5}} \, \psi^{ij} \phi_i \, \hat{\mathcal{H}}_{1j} + H.c. \right], \end{aligned} \tag{4}$$

where the soft parameters $\{a, b\}$ are assumed to be of the same order as $m_{\bar{5}}^2$ and m_{10}^2, and hence of $\mathcal{O}(M_{weak})$.

2.2 Boundary conditions at M_{in}

The no-scale structure (1) requires that all supersymmetry-breaking soft masses and bi- and tri-linear terms for the fields Φ_i vanish at M_{in}, so that

$$m_0 = B_0 = A_0 = 0, \tag{5}$$

where the bilinear couplings b_Σ and b_H in (4) are related to the corresponding superpotential terms by

$$b_\Sigma \; \equiv \; B_\Sigma \mu_\Sigma, \quad b_H \; \equiv \; B_H \mu_H. \tag{6}$$

and the trilinear couplings a', a, a_{10} and $a_{\bar{5}}$ in Eq (4) are related to the corresponding Yukawa couplings by

$$a' \equiv A'\lambda', \quad a \equiv A\lambda, \quad (a_{10})_{ij} \equiv A_{10ij}(h_{10})_{ij}, \quad (a_{\bar{5}})_{ij} \equiv A_{5ij}(h_{\bar{5}})_{ij}, \tag{7}$$

where no summation over repeated indices is implied. Having specified the boundary conditions on scalar masses as well as setting $A_0 = B_0 = 0$, we no longer have the freedom of choosing $\tan\beta$ as a free parameter. Instead, the minimization of the Higgs potential provides the solutions for both the MSSM Higgs mixing parameter μ and $\tan\beta$ [20]. Thus the theory is defined by 4 parameters:

$$m_{1/2},\ M_{in},\ \lambda,\ \lambda', \tag{8}$$

where we will denote the gaugino mass above the GUT scale by M_5. In addition, the sign of the MSSM μ parameter must also be specified [1].

2.3 Boundary conditions at $M_{\rm GUT}$

In the previous subsection, we specified the boundary conditions on the soft supersymmetry-breaking parameters at the input universality scale M_{in}. Using the GUT RGEs, these are run down to M_{GUT} where they must be matched with their MSSM equivalents. At the GUT scale, we have

$$\begin{array}{ll} M_i = M_5, & \\ m_D^2 = m_L^2 = m_{\bar{5}}^2, & a_t = 4a_{10}, \\ m_Q^2 = m_U^2 = m_E^2 = m_{10}^2, & a_b = a_\tau = a_{\bar{5}}/\sqrt{2}, \\ m_{H_d}^2 = m_{\mathcal{H}_1}^2, & m_{H_u}^2 = m_{\mathcal{H}_2}^2. \end{array} \tag{9}$$

We treat the gauge and Yukawa couplings differently, inputting their values at the electroweak scale and matching to their SU(5) counterparts at $M_{\rm GUT}$. The minimal SU(5) relations

$$h_E(M_{\rm GUT}) = h_D(M_{\rm GUT})^T, \tag{10}$$

between the charged-lepton and for the down-type Yukawa couplings are unrealistic since they do not produce the right values of lepton masses at $M_{\rm EW}$, except possibly for the third generation. We assume here that at $M_{\rm GUT}$

$$h_D(M_{\rm GUT}) = h_{\bar{5}}(M_{\rm GUT})/\sqrt{2}, \tag{11}$$

but we do not match h_E to h_5 at $M_{\rm GUT}$. Instead we use the values that h_E should have at $M_{\rm GUT}$ in order to produce the observed lepton masses. One way to justify this assumption would be to allow the lepton sector to have additional, non-renormalizable couplings besides the minimal renormalizable $\bar{5}$ couplings [22], so at $M_{\rm GUT}$ one has

$$h_E(M_{\rm GUT}) = h_{\bar{5}}(M_{\rm GUT})^T/\sqrt{2} + \text{ other interactions}, \tag{12}$$

where these other interactions are too small to be important for the quark sector. Thus for the gauge and Yukawa couplings, we determine their SU(5) counterparts as

$$g_i = g_5,$$

[1] It is determined from μ_H, λ, and the vacuum expectation value of Σ [21].

$$h_t = 4h_{10},$$
$$(h_D + h_E)_{33}/2 = h_{\bar{5}33}/\sqrt{2},$$
$$h_D(M_{\rm GUT})_{ij} = h_{\bar{5}}(M_{\rm GUT})_{ij}/\sqrt{2},\ \forall\ \{i,j\} \text{ except } \{i,j\} = 33, \tag{13}$$

The corresponding experimental inputs for the Yukawa couplings at the weak scale are shown in Table 1.

	Mass values [GeV]	$m_f^{\overline{MS}}(M_Z)$[GeV]
m_t	$173.21 \pm 0.51 \pm 0.71$	171.46 ± 0.96
m_b	4.18 ± 0.03	2.85 ± 0.04
m_c	1.275 ± 0.025	0.63 ± 0.025
m_s	0.095 ± 0.005	0.059 ± 0.0033
m_d	$4.8^{+0.5}_{-0.3} \times 10^{-3}$	0.0028 ± 0.0004
m_u	$2.3^{+0.7}_{-0.5} \times 10^{-3}$	0.0013 ± 0.0005
m_e	$(0.51 \pm (1.1 \times 10^{-8})) \times 10^{-3}$	$(0.49 \pm (4.2 \times 10^{-8})) \times 10^{-3}$
m_μ	$(105.66 \pm (3.5 \times 10^{-6})) \times 10^{-3}$	$(102.72 \pm (9.2 \times 10^{-6})) \times 10^{-3}$
m_τ	$1.78 \pm (1.2 \times 10^{-4})$	$1.75 \pm (2 \times 10^{-4})$

Table 1: *Values of the fermion masses, in GeV, as appear in current edition of the PDG review [23]. The quoted quark mass values at M_Z were obtained with the program* `RunDec` *[24]. The values of the charged lepton masses were taken from [25].*

We use for our renormalization-group calculations the program `SSARD` [26], which computes the sparticle spectrum on the basis of 2-loop RGE evolution for the MSSM and 1-loop evolution for minimal SU(5). We define M_{GUT} as the scale where $g_1 = g_2$, so that $M_{GUT} \simeq 10^{16}$ GeV, with its exact value depending on the values of other parameters. The value of g_3 at M_{GUT} is within the threshold uncertainties in the GUT matching conditions.

2.4 Non-zero off-diagonal Yukawa couplings

It is well known that renormalisation interrelates the soft masses-squared, trilinear and Yukawa couplings. In particular, a non-zero diagonal soft mass-squared term, the Kähler potential, the F terms and the Yukawa couplings could be seeds for non-zero off-diagonal soft masses-squared and trilinear terms. Alternatively, even if the Yukawa couplings were flavor-diagonal, there would be non-diagonal soft masses-squared and trilinear terms if the Kähler potential [9] or the F terms were flavor non-diagonal.

However, in the case of no-scale supergravity boundary conditions at M_{in} there is no source of non-zero trilinear or soft masses-squared, apart from the running induced by the renormalization-group β functions. However, off-diagonal Yukawa couplings at M_{in} would generate, via renormalization-group running, off-diagonal soft masses-squared and trilinear terms. The ultimate goal of our study is to quantify how large these parameters could be near M_{in} before they become problematic at $M_{\rm EW}$.

In order to understand the effects of the Yukawa couplings on the evolution of the soft supersymmetry-breaking parameters, we initialize our study by enforcing conditions at $M_{\rm EW}$ that reproduce the CKM matrix. In particular, we take the values of the quark masses at $M_{\rm EW}$ to be those at M_Z (see the second column of Table 1), and use $h_D(M_Z) = \sqrt{2}\, m_D(M_Z)/v/\cos\beta$ and $h_U(M_Z) = \sqrt{2}\, m_U(M_Z)/v/\sin\beta$. The diagonalization of the Yukawa couplings is defined by

$$h_D = V_R^D \hat{h}_D V_L^{D\dagger}, \quad h_E = V_R^E \hat{h}_E V_L^{E\dagger}, \tag{14}$$

where $\hat{h}_D$ and $\hat{h}_E$ are diagonal matrices, and the unitary matrices $V_{L,R}^{D,E}$ are such that the CKM matrix is $V_L^{U\dagger} V_L^D$.

Since the structure of the Yukawa couplings cannot be determined in a model-independent way, we adopt the minimal assumption that the CKM matrix is the only source of flavor violation in the Yukawa couplings in the D sector, and study the differences induced by different assumptions for the E sector. Thus, we are assuming that h_U is diagonal at $M_{\rm EW}$. Using this condition, 1-loop running does not generate off-diagonal terms, and the off-diagonal entries generated at $M_{\rm GUT}$ at the 2-loop level are negligibly small.

We remind the reader that, in contrast to the Standard Model, the MSSM observables are sensitive to right-handed currents, which have no Standard Model counterparts. Therefore, it is not possible to make predictions without additional assumptions [2] on the Yukawa couplings, and hence the $V_R^{D,E}$ as well as the $V_L^{D,E}$.

We therefore consider the following illustrative Ansätze that illustrate the range of possibilities:

$$A1. \quad V_R^{D*} = V_L^D = V_{\rm CKM}, \qquad V_R^E = V_L^E = 1, \tag{15}$$

$$A2. \quad V_L^D = V_{\rm CKM}, \quad V_R^D = 1, \quad V_R^E = V_L^E = 1, \tag{16}$$

$$A3. \quad V_R^D = V_L^E = 1, \qquad V_L^D = V_R^{E*} = V_{\rm CKM}, \tag{17}$$

$$A4. \quad V_R^{D*} = V_L^D = V_{\rm CKM}, \qquad V_R^{E*} = V_L^E = V_{\rm CKM}. \tag{18}$$

The Ansätze A3 and A4 are compatible with the minimal SU(5) conditions (10) and (14). However, we will focus later on Ansätze A1 and A2 because, as we shall see, Ansätze A3 and A4 give rise to unacceptably large flavour-violating processes in the lepton sector. We use examples A1 and A2 to illustrate the determination of the diagonal and off-diagonal soft masses-squared and trilinear terms that are generated below M_{in}. These are constrained by flavour observables, and our goal is to determine how large the deviations from pure no-scale boundary conditions can be, before they induce flavour violations in contradiction with experiment.

3 Running of Parameters

In this Section, we restrict our attention to pure no-scale boundary conditions, and assume the Ansatz A1 for the CKM mixing among fermions. As already mentioned, the boundary conditions for the soft supersymmetry-breaking parameters are fixed at M_{in}, the gauge and Yukawa couplings are fixed at the weak scale, and all parameters are matched at M_{GUT} to allow for running above and below the GUT scale. Though the off-diagonal sfermion masses begin their RGE evolution with the no-scale boundary conditions, i.e., they vanish at M_{in}, they contribute to low-energy flavour observables in a model-dependent way after renormalisation, as we now calculate.

To be concrete, we choose a limited set of benchmark points with different choices of λ, λ' and M_{in} (all masses are expressed in GeV units). The 4-dimensional parameter space of the super-GUT no-scale model was explored in [14]. It was found that unless $\lambda/\lambda' < 0$ with $|\lambda| < |\lambda'|$, both $m_{1/2}$ and M_{in} are pushed to relatively low values. However, the low values of $m_{1/2}$ are now in conflict with LHC searches for supersymmetric particles [28]. Therefore

[2] Such assumptions can have important effects on the observables, and can help to determine the choices of Yukawa structures compatible with a given supersymmetric model [27].

we restrict our analysis to an illustrative benchmark point **B** defined by

$$\mathbf{B}: \quad M_5 = 1500 \text{ GeV}, \quad M_{in} = 1 \times 10^{18} \text{ GeV}, \quad \lambda' = 2, \quad \lambda = -0.1, \tag{19}$$

suggested by a no-scale model [15] in which the right-handed sneutrino is responsible for Starobinsky-like inflation. The value of M_5 is chosen so that we obtain the relic abundance corresponding to the cold dark matter density determined by Planck and other experiments [29]. As noted earlier, after setting $A_0 = B_0 = 0$, we no longer have the freedom of choosing $\tan\beta$ as a free parameter. For benchmark **B**, we find $\tan\beta \simeq 52$. The value of M_5 is large enough to satisfy LHC bounds from supersymmetric particle searches and the lightest Higgs mass is $m_h = 125.0 \pm 3.1$ GeV when calculated with the `FeynHiggs` code [30], which is comfortably consistent with the joint ATLAS and CMS measurement of m_h [31]. It is important to compare correctly theoretical predictions of $B_s \to \mu^+\mu^-$ with its experimental value, as was reviewed in [32]. In particular, one should compare the "untagged" computed value, instead of the tagged one, to its experimental counterpart. The relevance of this comparison for some supersymmetric scenarios was studied in [33], where it was pointed out that this difference is important for evaluating the validity of some scenarios. Using the `SUSY_FLAVOR` code [34] and the latest hadronic observables, we find that for the benchmark point under consideration the tagged value is 3.42×10^{-9}, whilst using a modified version of the `SUSY_FLAVOR` code we find that the untagged value is 3.76×10^{-9}. Because $\tan\beta$ is relatively high for this benchmark point, the branching ratio of $B_s \to \mu^+\mu^-$ is somewhat large, but within the experimental 95% CL upper limit [35].

3.1 Runnings of SU(5) parameters

As already emphasised, the soft supersymmetry-breaking mass parameters are zero at the input scale in a no-scale model, but running between M_{in} and M_{GUT} leads in general to non-zero masses for both diagonal and non-diagonal elements. In particular, the latter are induced by the non-diagonal Yukawa couplings assumed in Ansatz A1. The runnings of the Yukawa couplings for benchmark **B** are shown in Fig. 1. Recall that we have assumed diagonal Yukawa matrices for the up-quark sector and the **10** of SU(5), and therefore we show only the evolution of the real part of h_{10ii}. In contrast, for the $\bar{\mathbf{5}}$ of SU(5), the Yukawa matrices are determined from (14) using Ansatz A1. Note that, with this definition, these Yukawa matrices are in general not symmetric (though the runnings of $h_{5_{12}}$ and $h_{5_{21}}$ are indistinguishable in the figure). The Figure shows the runnings of the Yukawa couplings from the input scale M_{in} ($\ln(\mu/M_{GUT}) \approx 4.6$ for benchmark **B**) down to the GUT scale ($\ln(\mu/M_{GUT}) = 0$).

The running of the soft scalar masses is shown in Fig 2, where we have again assumed benchmark point **B** and ansatz A1. The top panels show the running of the diagonal soft masses for the **10** and $\bar{\mathbf{5}}$ of SU(5). The middle panels show the real parts of the off-diagonal entries, and the bottom panels show the imaginary parts of the same off-diagonal entries (as these are hermitian quantities, information on the transposed entries are already given by the real and imaginary parts). All of the squark masses begin their evolution with $m^2 = 0$ at M_{in}. The running of the diagonal components is driven by the value of the gaugino mass, here set at $M_{1/2} = 1500$ GeV. We clearly see from Fig 2 that the off-diagonal elements of the squark mass matrices induced by the non-diagonal Yukawa matrices remain very small after we have imposed the no-scale boundary conditions: we find $(m^2_{\bar{5}})_{12}, (m^2_{\mathbf{10}})_{12} \ll (m^2_{\bar{5}})_{13} \approx (m^2_{\mathbf{10}})_{13} \approx -20$ GeV^2, $(m^2_{\bar{5}})_{23} \approx -1100$ GeV^2, $(\mathrm{m}^2_{\mathbf{10}})_{23} \approx -550$ GeV^2, while $(m^2_{\bar{5}})_{ii}$ and

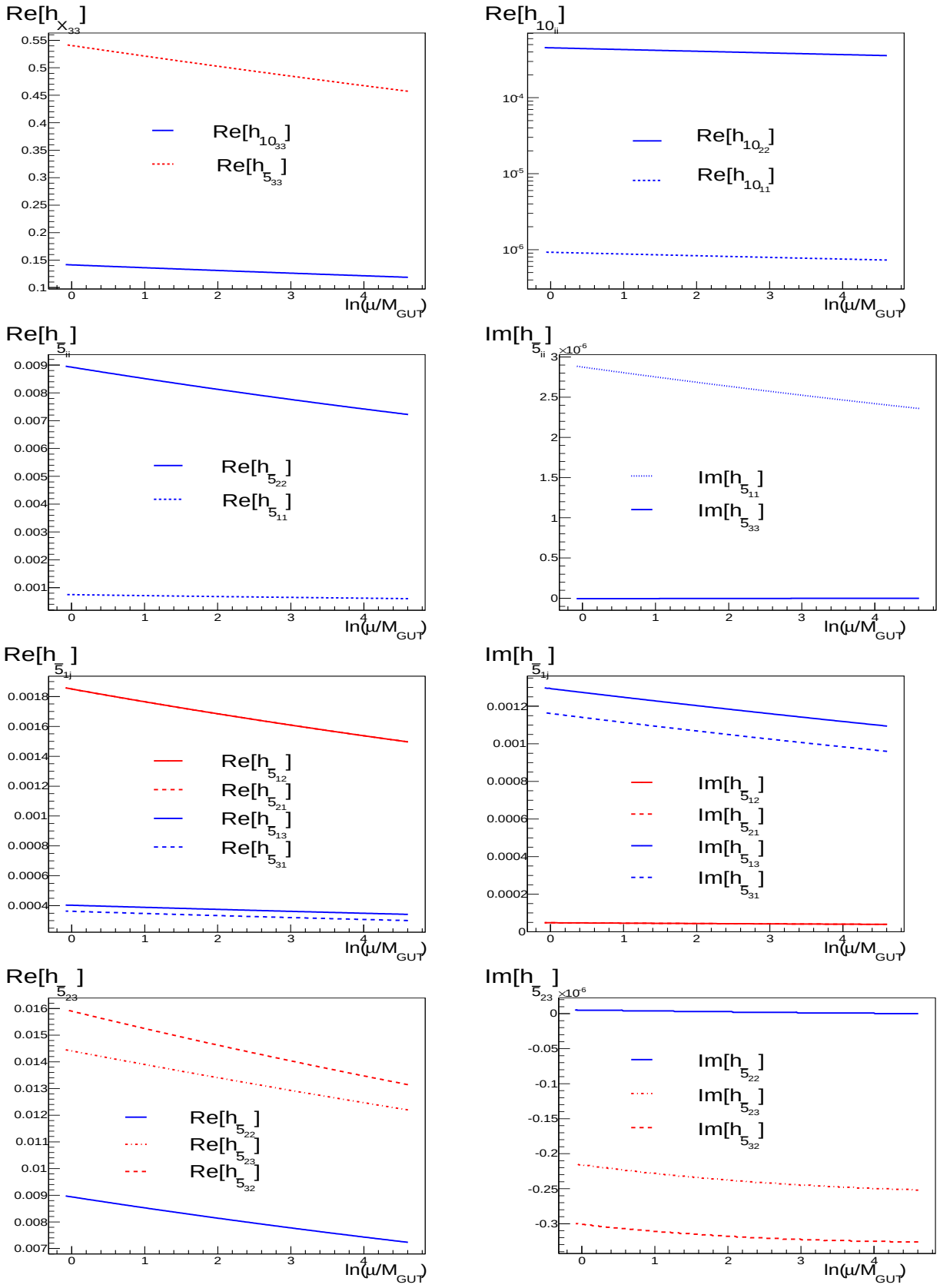

Figure 1: *The runnings of the Yukawa couplings from M_{in} to M_{GUT} for the benchmark point* **B**, *using the patterns specified via Ansatz A1. Note that the lines for $h_{\bar{5}_{12}}$ and $h_{\bar{5}_{21}}$ lie on top of each other.*

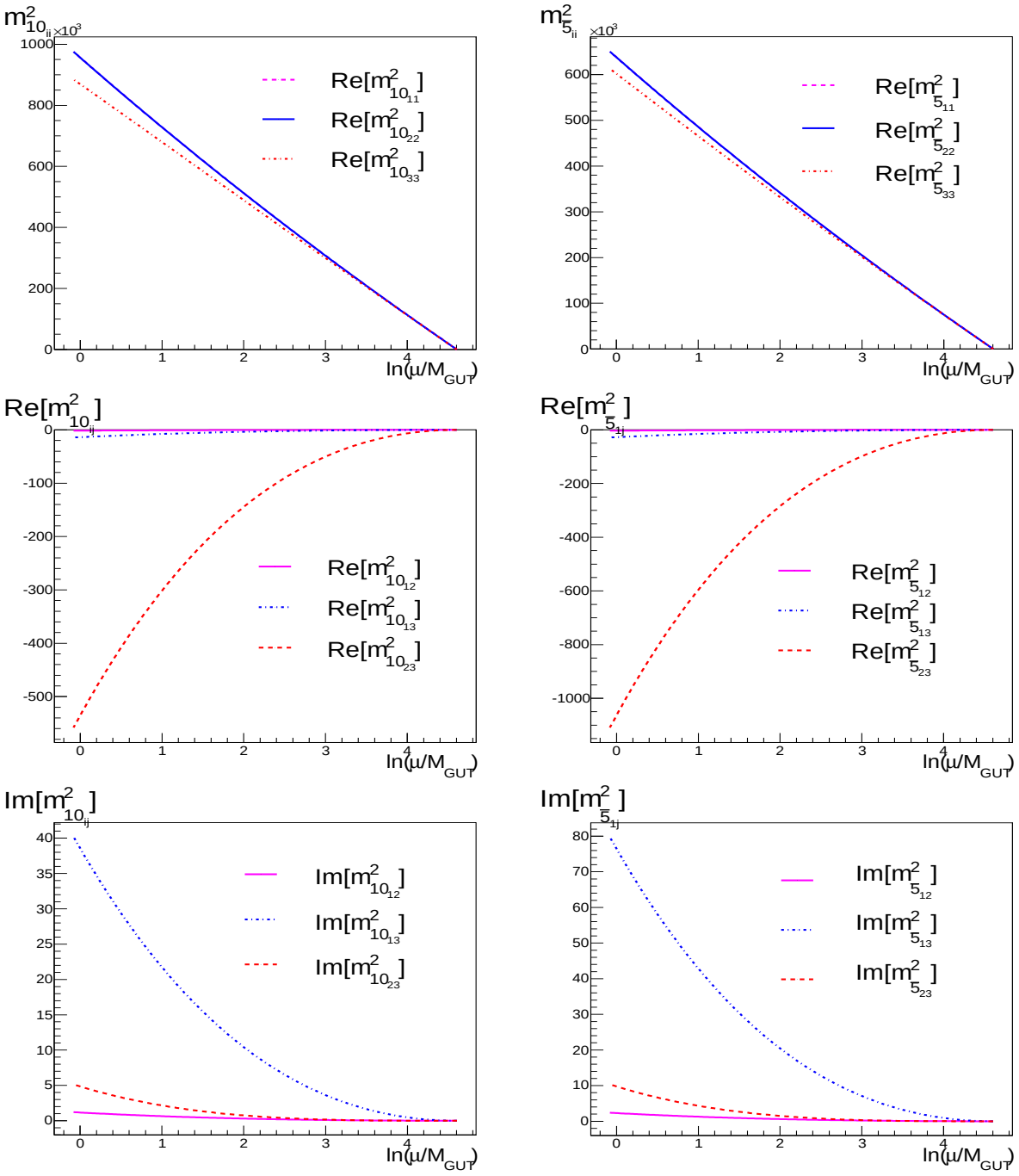

Figure 2: *The runnings of diagonal (left) and off-diagonal (right) soft masses-squared associated with the* **10** *(left) and* $\overline{\mathbf{5}}$ *(right) representations in the SU(5) model between* M_{in} *and* M_{GUT} *for the benchmark point* **B** *(in units of* GeV^2*) using Ansatz A1 for the Yukawa couplings.*

$(m^2_{\mathbf{10}})_{ii}$ are of order 10^5 and 10^6 GeV^2, respectively. Later we will use this evolution to place constraints on the size of the possible sizes of the off-diagonal elements at M_{in}.

3.2 Running of MSSM parameters

The matching of couplings and masses at M_{GUT}, using Eq (9), is made in the basis where the Yukawa couplings are not diagonal, i.e., we assume ansatz A1. The transformations to

the super-CKM (SCKM) basis, where the Yukawa couplings are diagonal, are given by

$$\begin{aligned}
\hat{m}^2_{D(LL)} &= V_L^{D\dagger} m_Q^2 V_L^D, \\
\hat{m}^2_{E(LL)} &= V_L^{E\dagger} m_L^2 V_L^E, \\
\hat{m}^2_{f(RR)} &= V_R^{f\dagger} m_f^2 V_R^f, \quad f = D, E, \\
\hat{m}^2_{f(LR)} &= -\hat{a}_f v_f + \mu \tan\beta \; \hat{m}_{f_i} \delta_{ij}, \\
\hat{a}_f &= V_L^{f\dagger} a_f V_R^f, \quad f = D, E,
\end{aligned} \tag{20}$$

where the matrices $V_X^{f\dagger}$ $(X = L, R)$ are defined in (14) and the $\hat{m}_{f_i}$ are the fermion masses, $i = 1, 2, 3$. We could also define $\hat{m}^2_{U(LL)} = V_L^{U\dagger} m_Q^2 V_L^U$, but we are taking V_L^U to be diagonal. We note that $SU(2)_L$ invariance in the SCKM basis is preserved trivially, because then $m_Q^2 = V_L^D \hat{m}^2_{D(LL)} V_L^{D\dagger} = V_L^U \hat{m}^2_{U(LL)} V_L^{U\dagger}$ and so $\hat{m}^2_{U(LL)} = V_{\rm CKM} \hat{m}^2_{D(LL)} V_{\rm CKM}^\dagger$. A more complete set of transformation rules are given in Appendix B. The choice of Ansatz in Eqs. (15) to (18) induces off-diagonal entries at M_{GUT} in the SCKM basis, which are constrained by flavor-violating processes. In particular, for Ansätze 3 and 4, we find that BR$(\mu \to e\gamma)$ is too large and, in addition, for Ansatz 4 some electric dipole moments (EDMs) are too large. On the other hand, both the Ansätze A1 and A2 induce acceptable amounts of flavor violation. Ansatz 1 is interesting because both the right- and left-diagonalization matrices $V_{L,R}$ are CKM-like. We plot the runnings of the MSSM soft-squared parameters for this Ansatz in Figs. 3 to 5.

We plot in the first panel of Fig. 3 the running of some squark soft masses-squared. The horizontal axis is $x = \ln(\mu/M_{GUT})$, and the red curves represent the evolution of states in the basis where Yukawa couplings *are not* diagonal. That is, starting with our boundary conditions: $m_0 = 0$ at $x \simeq 4.6$, the sfermion masses are run down to M_{GUT} where they are matched to the MSSM sfermion masses. As the running to M_{GUT} has induced some off-diagonal entries, these are also run down to the weak scale ($x \simeq -32$). This running is shown by the set of red curves. For example, at the electroweak scale, the running of the diagonal left-handed squark masses-squared $m^2_{Q_{33}}$ reaches 11×10^6 GeV^2, while $m^2_{Q_{ii\neq 3}}$ reaches 14×10^6 GeV^2 . The split between the first and second generation is not appreciable on the scale displayed on the plot. We can diagonalize the mass matrices at the weak scale using Eq. (20) with the V's defined by A1. That result is shown by the blue crosses. In the upper left panel it makes no difference whether we run in the diagonal (SCKM) basis Eq (20) or in the non-diagonal Yukawa basis, as the blue crosses sit at the endpoint of the red curves.

In the second to sixth panels, we show the running of $m^2_{Q_{23}}$, $m^2_{D_{ii}}$, $i = 1, 2, 3$, m^2_{D23}, $m^2_{U_{ii}}$, $i = 1, 2, 3$, and m^2_{U23}. We again show as blue crosses the endpoints of the running at the weak scale when the states are in the basis where Yukawa couplings are diagonal. The positions of these show the impact of the changes in size of off-diagonal parameters. We see that the blue crosses differ only slightly from the running shown by the red curves for the imaginary parts of Q_{23} and D_{23}. Since the Yukawa couplings are chosen to be diagonal for U, the blue crosses are found at the endpoints of the red curves in these cases.

In Figs. 4 and 5 we show the same for the runnings of $m^2_{L_{ii}}$, $i = 1, 2, 3$, m^2_{L23}, m^2_{L12}, $m^2_{E_{ii}}$, $i = 1, 2, 3$, m^2_{E12}, $m^2_{Q_{12}}$, m^2_{D12} and $m^2_{f_{13}}$, $f = Q, D, L, E$. We do not show the runnings of m^2_{E23}, m^2_{U12} and m^2_{U13} because, given the matching conditions at M_{GUT}, Eq (9), and the fact that in the E and U sectors the Yukawa couplings are chosen to be diagonal, their runnings are similar to m^2_{U23}, m^2_{E12} and m^2_{E13}, respectively.

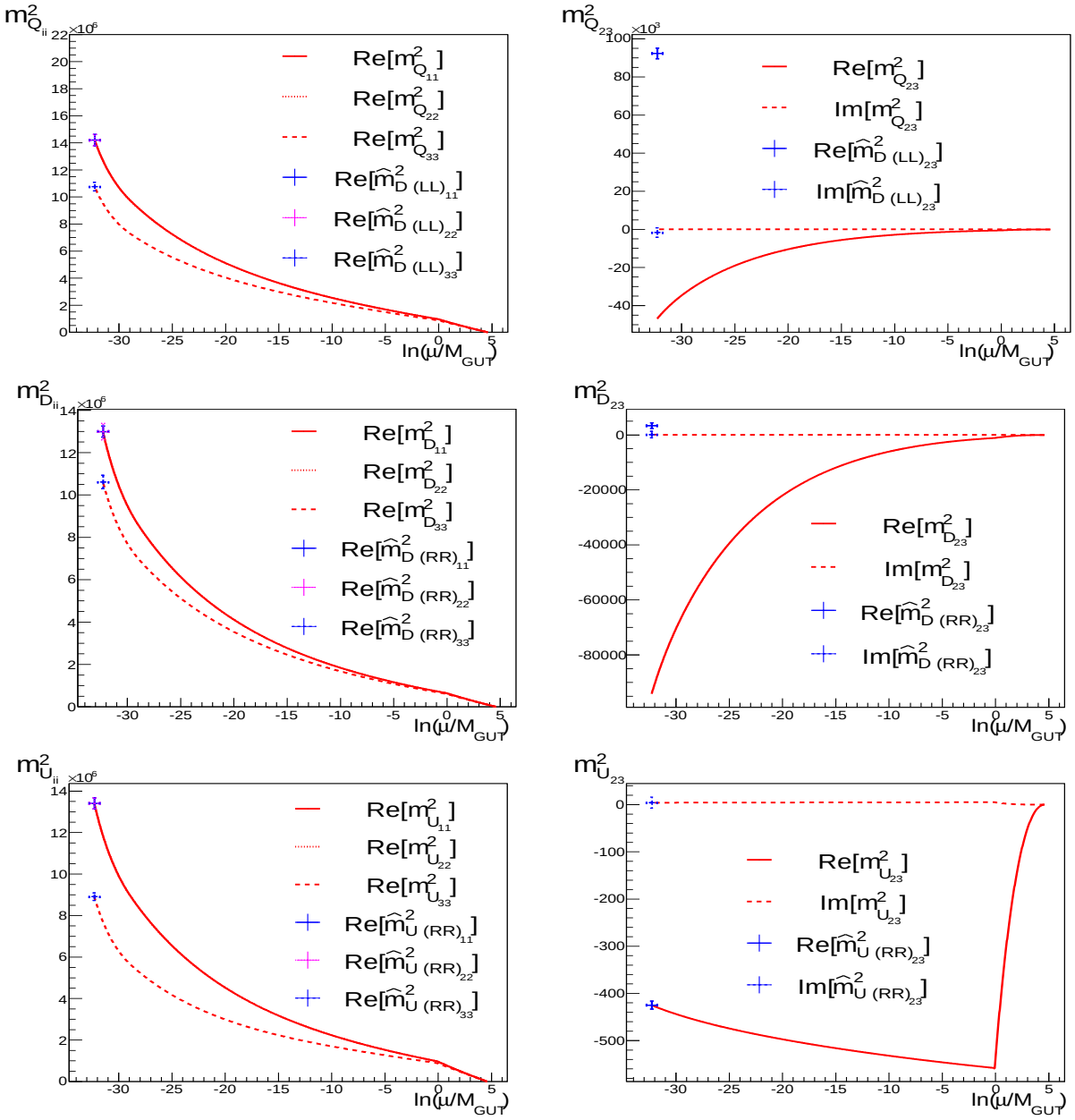

Figure 3: *The runnings of soft-squared masses for the MSSM parameters for Ansatz A1. The horizontal axis is* $\ln(\mu/M_{GUT})$*, and the vertical axis shows the mass-squared in units of [GeV]*^{2}*. For the diagonal soft-squared masses, the split between first and second generation is not appreciable on the scale of the plot. In each panel we show the runnings of* $m^2_{Q_{ii}}$*,* $i = 1,2,3$*,* $m^2_{Q_{23}}$*,* $m^2_{D_{ii}}$*,* $i = 1,2,3$*,* m^2_{D23}*,* $m^2_{U_{ii}}$*,* $i = 1,2,3$ *and* m^2_{U23}*. The red lines in the plots run from the input scale,* M_{in}*, down to* $M_{\rm EW}$ *(with the appropriate matching at* $M_{\rm GUT}$*) and are given in the basis where Yukawa couplings are not diagonal. The blue crosses show the result (at the electroweak scale) of running in the basis where the Yukawa matrices are diagonal. The states labeled without a hat are the states given in the basis where Yukawa couplings are not diagonal. The SU(5) parameters were specified in the basis where the Yukawa couplings are not diagonal.*

As one can see in Figs. 4 and 5, there is considerably less running for the (12) components of the squark mass matrices. For the (13) sectors, looking at Fig. 5, we find that, depending on the sector, the running can be more or less important. As expected for m^2_{E13}, the running is negligible because in this sector the Yukawa couplings are chosen to be diagonal. Note that, due to the CP violating phase of the CKM, the running of the imaginary parts of m^2_{D13}

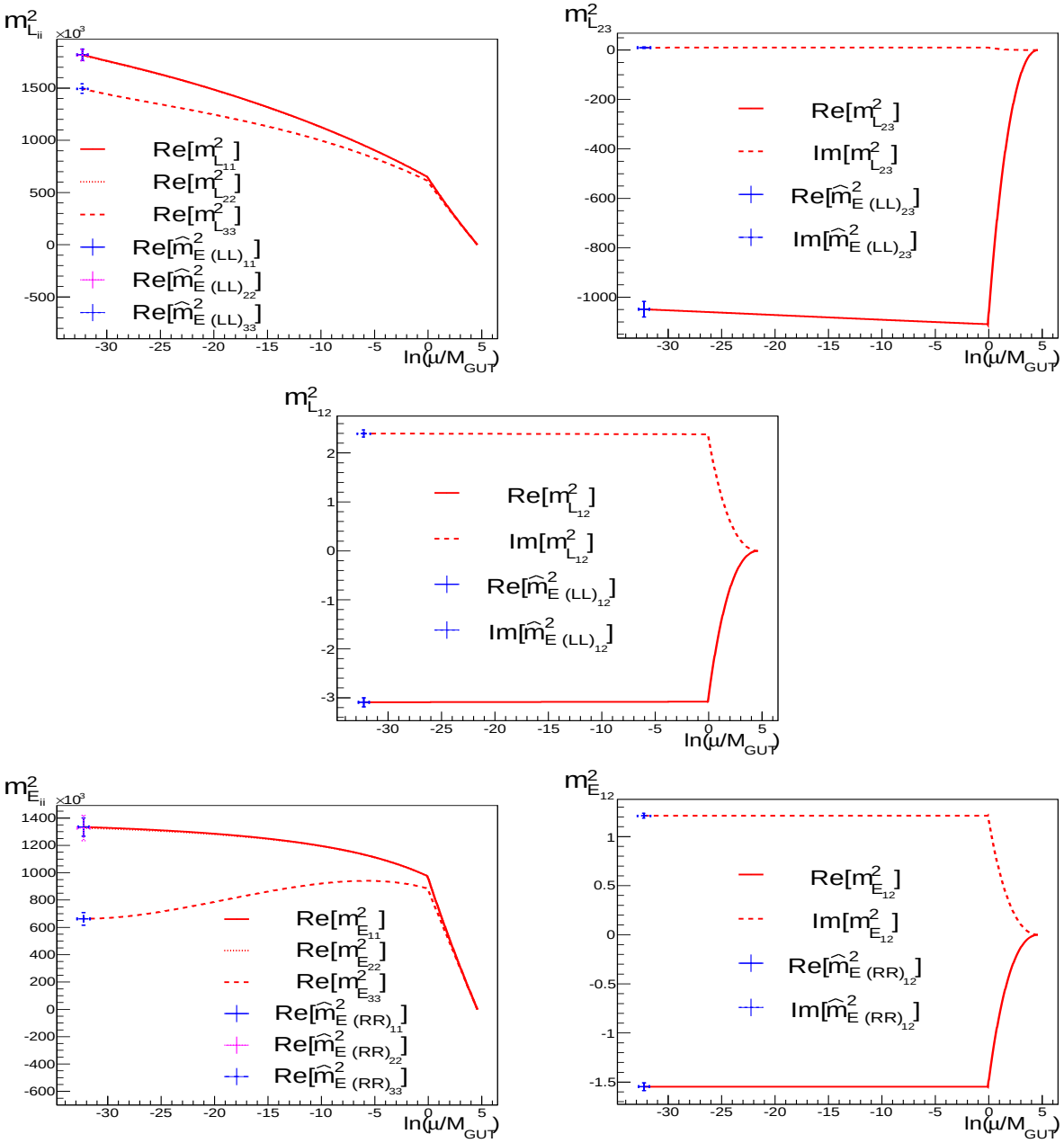

Figure 4: *As in Fig 3, but for* m^2_{Lii}, $i = 1, 2, 3$, m^2_{L23}, m^2_{L12}, m^2_{Eii}, $i = 1, 2, 3$, *and* m^2_{E12}. *The horizontal axis is again* $\ln(\mu/M_{GUT})$.

and m^2_{L13} become appreciable. In the D sector, however, once the SCKM transformations, Eq (20), are taken into account, some of the CP violation is rotated away, as a result of the first condition of Ansatz 1, Eq (15).

3.3 Flavor-violating parameters

We define the flavor-violating parameters

$$(\delta^f_{ij})_{\{XY\}} \equiv \frac{\hat{m}^2_{f(XY)_{ij}}}{\sqrt{\hat{m}^2_{f(XX)_{ii}} \hat{m}^2_{f(YY)_{jj}}}}, \quad f = D, E, \tag{21}$$

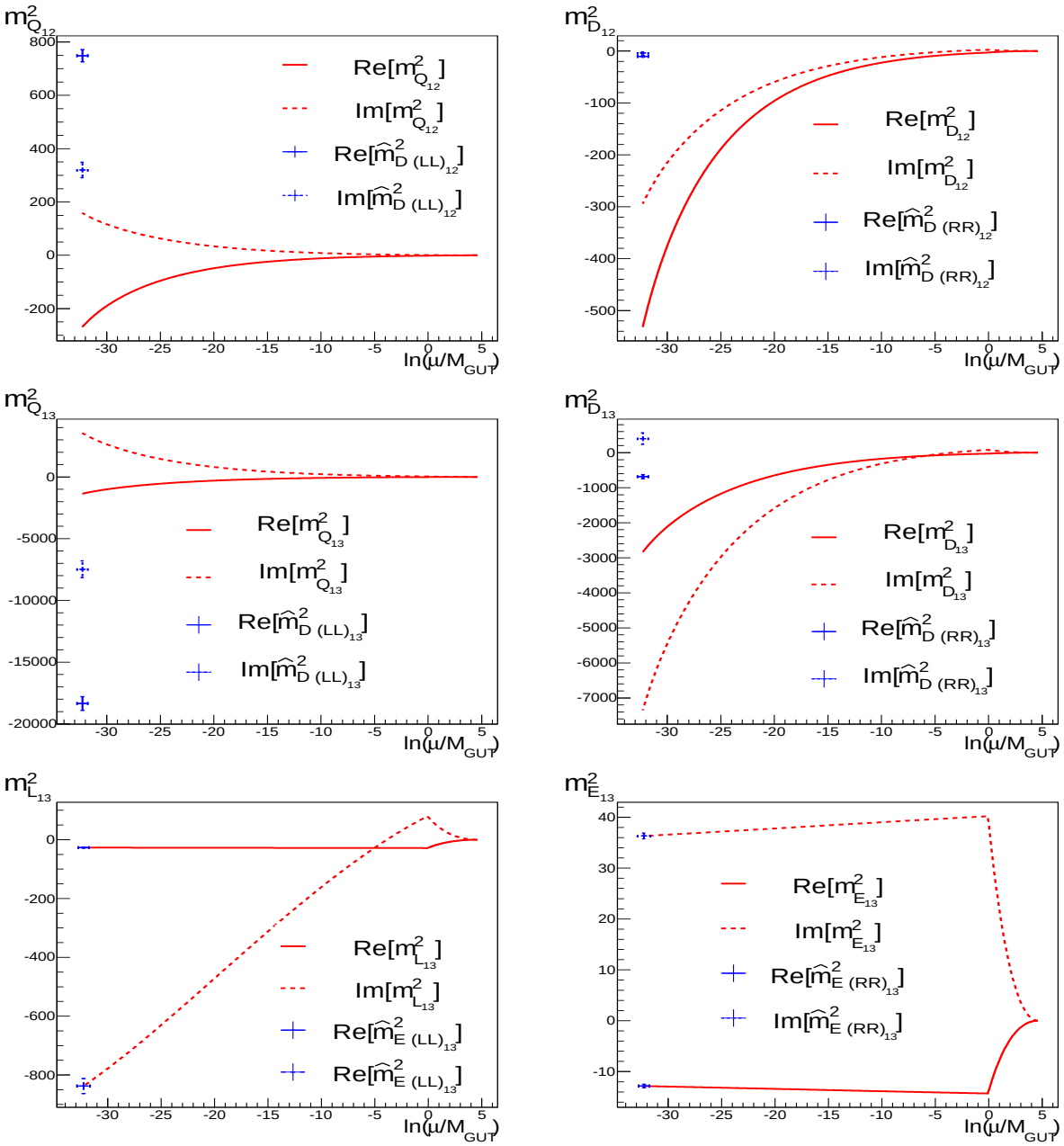

Figure 5: *As in Fig 4 but now for* m^2_{Q12}, m^2_{D12} *and* m^2_{f13}, $f = Q, D, L, E$. *The horizontal axis is again* $\ln(\mu/M_{GUT})$.

where the mass matrices appearing on the right-hand side of the equation are defined in Eq (20) and $X = L, R$. Flavor-violating parameters are often defined in the absence of a particular model in which the running can be performed explicitly. However, general limits on flavor-violating parameters cannot be obtained, because the forms in which they enter into observables are in general quite model-dependent, see for example [36] and [37]. There are dependences both on the mass scales of the supersymmetric particles involved in a particular process - in a particular model not all the supersymmetric particles may be relevant - and on the specific underlying flavor framework. However, a few observables can severely constrain the parameters of Eq (21) and give clean bounds on them, particularly for the sleptonic parameters. They still depend on the mass scale and assumptions of the underlying flavor model, but can be used as an indication, provided the model satisfies

the conditions under which the bounds are derived. In particular, in [38] we find a set of conditions compatible with our assumptions, and we use them to compare to the lepton-flavour-violating parameters of Eq (21).

The main purpose here in using the parameters of Eq (21) is to compare our different models and to examine the different runnings and the contributions from the different sectors to a particular observable. Using the bounds of [38], we make comparisons and comment on cancellations in the models.

Comparison between A1 and A2

The only difference between A1 and A2 is in the D-quark sector, Eqs. (15-18), so we concentrate our comparison on the D-squark sector (left and right). Our interest in comparing these Ansätze is to assess the relevance of switching off (A2) the effect of the CKM matrix in the right-handed D sector, and to check potential differences in the observables. The runnings of the flavor-violating parameters from the GUT scale to the weak scale is shown in Figs. 6 and 7 for models A1 and A2. At $M_{\rm GUT}$, the initial values for most of the δ parameters are quite similar for both these Ansätze. In some cases the sign differs, but they have a comparable absolute value.

The parameters that differ the most are the LR flavor-violating parameters in the (13) flavour sector, as can be seen from Tables 2 and 3. The behaviors of the real and imaginary parts are plotted in Fig. 7, notice the different scales of the plots. The differences between Ansätze A1 and A2 are to be expected, as they arise from the different choices for V_R^D. Looking at the terms that enter into the beta function of a_D, shown in Eq (37) in Appendix B, we see that all terms involving a_D are sensitive to the change of V_R^D, which affect directly the LR parameters. In contrast, we see from Eq (36) of Appendix B that only some of the soft mass-squared transformations that contribute to the LL and RR parameters are sensitive to the choice of V_R^D. As a result, we do not expect the flavor-violating parameters coming entirely from the soft masses-squared to be very sensitive to the change of V_R^D. Indeed, looking at Tables 2 and 3, we see that the difference is at most one order of magnitude in the (13) RR and LL sectors for A1 and A2. In the (12) sector, we again see the strong dependence on V_R^D in the LR parameters and relatively small changes in the RR and LL parameters. In the (23) sector, none of the terms are greatly affected by the choice of V_R^D. Because of the difference between the Yukawa couplings $h_{D_{23}}$ and $h_{D_{32}}$, the parameters $a_{D_{23}}$ and $a_{D_{32}}$ will have different values at the EW scale, but their absolute values are similar because their runnings are dominated by the largest Yukawa coupling, i.e., terms $\propto \hat{h}^2_{D_3}$ in Eq (37), and contain $V^{D\dagger}_{L,Rii}$ elements. This is not the case for the lighter sectors, because their Yukawa couplings are smaller. By way of comparison, we plot the runnings of some of the (12) flavor parameters in Fig. 6.

Due to the running of the a_D beta function due in particular to the third and fourth terms in Eq (37), a_D will not evolve symmetrically even if h_D is symmetric, and therefore

$$\begin{aligned} \mathrm{Re}[(\delta^D_{ij})_{RL}] &\neq \mathrm{Re}[(\delta^D_{ji})_{RL}]\,, \\ \mathrm{Im}[(\delta^D_{ij})_{RL}] &\neq \mathrm{Im}[(\delta^D_{ji})_{RL}]\,. \end{aligned} \tag{22}$$

If, in addition, h_D is not symmetric (as in Ansatz A2), this effect can be quite noticeable (in particular for $(\delta^D_{12})_{RL}$, $(\delta^D_{21})_{RL}$, $(\delta^D_{13})_{RL}$ and $(\delta^D_{31})_{RL}$). However, the behaviors of the other flavor-violating parameters tells us that their evolutions in the SCKM basis do not differ too much, which is explained by the forms of the transformations in Eq (36), so we have not

plotted them in Figs. 6 and 7. The order-of-magnitude differences in the real and imaginary parts of $(\delta^f_{ij})_{\{XY\}}$ are given in Tables 2 and 3, respectively.

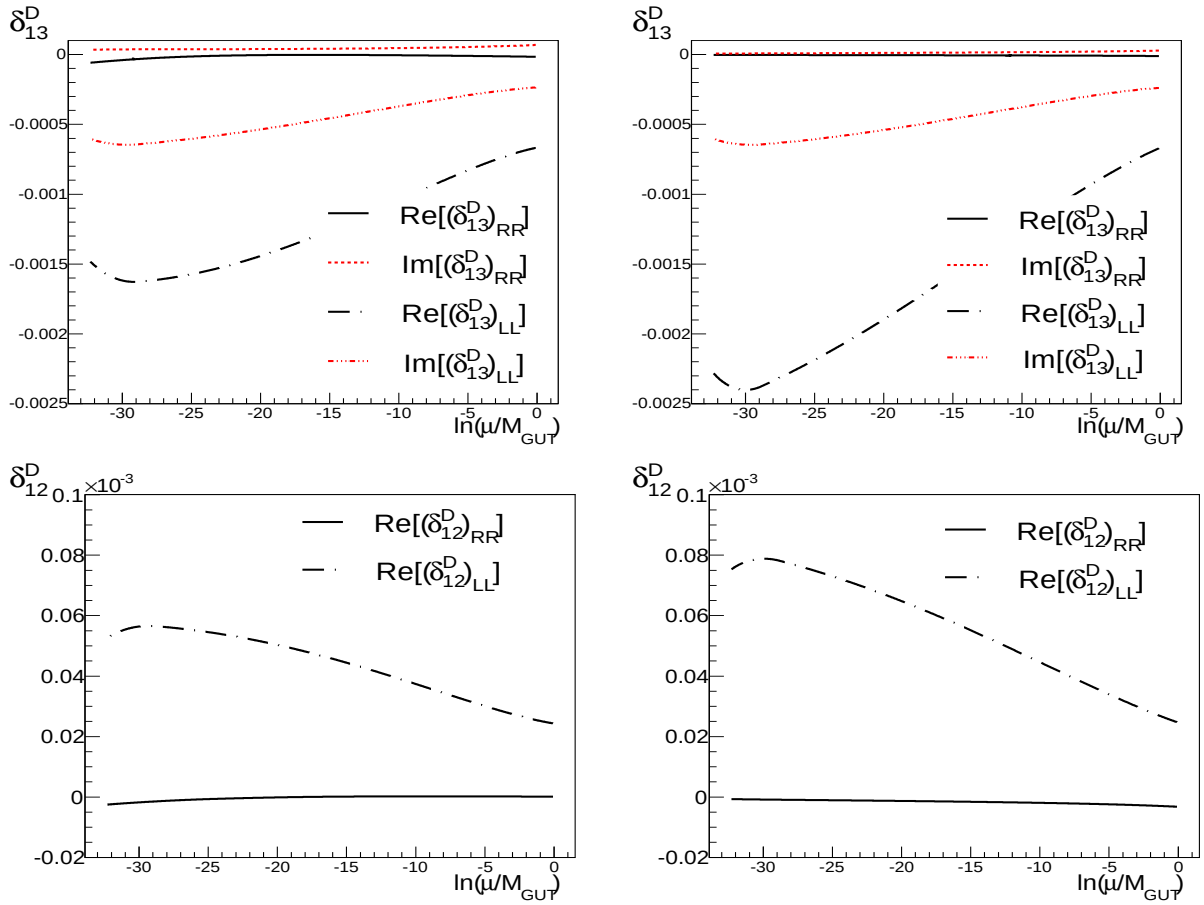

Figure 6: *Comparison of the runnings of the D-quark flavor-violating parameters δ for A1 (left panels) and A2 (right panels), for $(\delta^D_{1i})_{\{XX\}}$, $i = 2, 3$, $X = L, R$.*

	A1	A2	Bound (Process) [39]
$\mathrm{Re}[(\delta^{\mathrm{D}}_{12})_{\mathrm{RR}}]$	-8×10^{-7}	-2×10^{-7}	10^{-2} (ΔM_K)
$\mathrm{Re}[(\delta^{\mathrm{D}}_{12})_{\mathrm{LL}}]$	5×10^{-5}	8×10^{-5}	10^{-2} (ΔM_K)
$\mathrm{Re}[(\delta^{\mathrm{D}}_{12})_{\{\mathrm{LR,RL}\}}]$	3×10^{-7}	-5×10^{-11}	-
$\mathrm{Re}[(\delta^{\mathrm{D}}_{21})_{\{\mathrm{LR,RL}\}}]$	3×10^{-7}	3×10^{-7}	-
$\mathrm{Re}[(\delta^{\mathrm{D}}_{13})_{\mathrm{RR}}]$	-6×10^{-5}	-2×10^{-6}	-
$\mathrm{Re}[(\delta^{\mathrm{D}}_{13})_{\mathrm{LL}}]$	-1×10^{-3}	-2×10^{-3}	-
$\mathrm{Re}[(\delta^{\mathrm{D}}_{13})_{\{\mathrm{LR,RL}\}}]$	5×10^{-7}	9×10^{-10}	-
$\mathrm{Re}[(\delta^{\mathrm{D}}_{31})_{\{\mathrm{LR,RL}\}}]$	-5×10^{-7}	-5×10^{-7}	-
$\mathrm{Re}[(\delta^{\mathrm{D}}_{23})_{\mathrm{RR}}]$	3×10^{-4}	-8×10^{-3}	10^{-2} $(\mathrm{BR}(B_s \to \mu^+\mu^-))$
$\mathrm{Re}[(\delta^{\mathrm{D}}_{23})_{\mathrm{LL}}]$	7×10^{-3}	1×10^{-2}	10^{-2} $(\mathrm{BR}(B_s \to \mu^+\mu^-))$
$\mathrm{Re}[(\delta^{\mathrm{D}}_{23})_{\{\mathrm{LR,RL}\}}]$	-2×10^{-6}	-3×10^{-6}	-
$\mathrm{Re}[(\delta^{\mathrm{D}}_{32})_{\{\mathrm{LR,RL}\}}]$	2×10^{-6}	2×10^{-6}	-

Table 2: *Comparison of the real parts of the D-squark parameters $(\delta^f_{ij})_{\{XY\}}$ in Ansätze A1 and A2.*

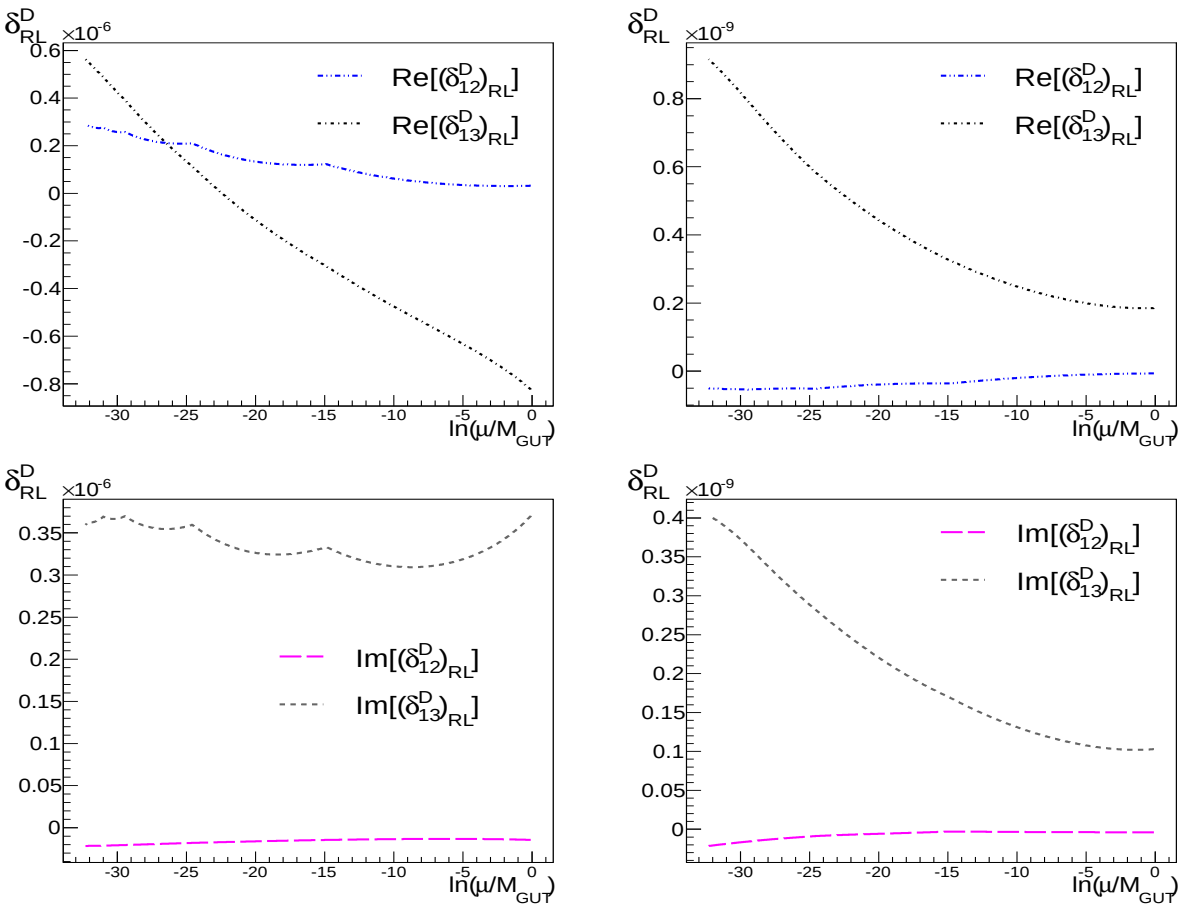

Figure 7: *Comparison of the runnings of the D-quark flavor-violating parameters δ for A1 (left panels) and A2 (right panels), for $(\delta^D_{1i})_{LR}$, $i = 2, 3$.*

	A1	A2
$\mathrm{Im}[(\delta^{\mathrm{D}}_{12})_{\mathrm{RR}}]$	-3×10^{-7}	2×10^{-7}
$\mathrm{Im}[(\delta^{\mathrm{D}}_{12})_{\mathrm{LL}}]$	2×10^{-5}	3×10^{-5}
$\mathrm{Im}[(\delta^{\mathrm{D}}_{12})_{\{\mathrm{LR,RL}\}}]$	-2×10^{-8}	-2×10^{-11}
$\mathrm{Im}[(\delta^{\mathrm{D}}_{21})_{\{\mathrm{LR,RL}\}}]$	5×10^{-9}	1×10^{-8}
$\mathrm{Im}[(\delta^{\mathrm{D}}_{13})_{\mathrm{RR}}]$	3×10^{-5}	6×10^{-6}
$\mathrm{Im}[(\delta^{\mathrm{D}}_{13})_{\mathrm{LL}}]$	-6×10^{-4}	-6×10^{-4}
$\mathrm{Im}[(\delta^{\mathrm{D}}_{13})_{\{\mathrm{LR,RL}\}}]$	4×10^{-7}	4×10^{-10}
$\mathrm{Im}[(\delta^{\mathrm{D}}_{31})_{\{\mathrm{LR,RL}\}}]$	-1×10^{-8}	-1×10^{-8}
$\mathrm{Im}[(\delta^{\mathrm{D}}_{23})_{\mathrm{RR}}]$	1×10^{-5}	2×10^{-6}
$\mathrm{Im}[(\delta^{\mathrm{D}}_{23})_{\mathrm{LL}}]$	-1×10^{-4}	-1×10^{-4}
$\mathrm{Im}[(\delta^{\mathrm{D}}_{23})_{\{\mathrm{LR,RL}\}}]$	8×10^{-8}	3×10^{-9}
$\mathrm{Im}[(\delta^{\mathrm{D}}_{32})_{\{\mathrm{LR,RL}\}}]$	-5×10^{-8}	-5×10^{-8}

Table 3: *Comparison of the imaginary parts of the D-squark parameters $(\delta^f_{ij})_{\{XY\}}$ in Ansätze A1 and A2. The bounds on the imaginary parts in these scenarios cannot be taken directly from the literature, but must instead be constructed from different observables (see Section 3.4).*

Comparison between A1 and A4

The difference between A1 and A4 is due to the replacement of $V^{E*}_R = V^E_L = 1$ by

$V_R^{E*} = V_L^E = V_{\rm CKM}$, so we expect a significant increase in the leptonic L, R flavor-violating parameters, as they are directly linked to the trilinear couplings, which are enhanced by the running of the Yukawa couplings.

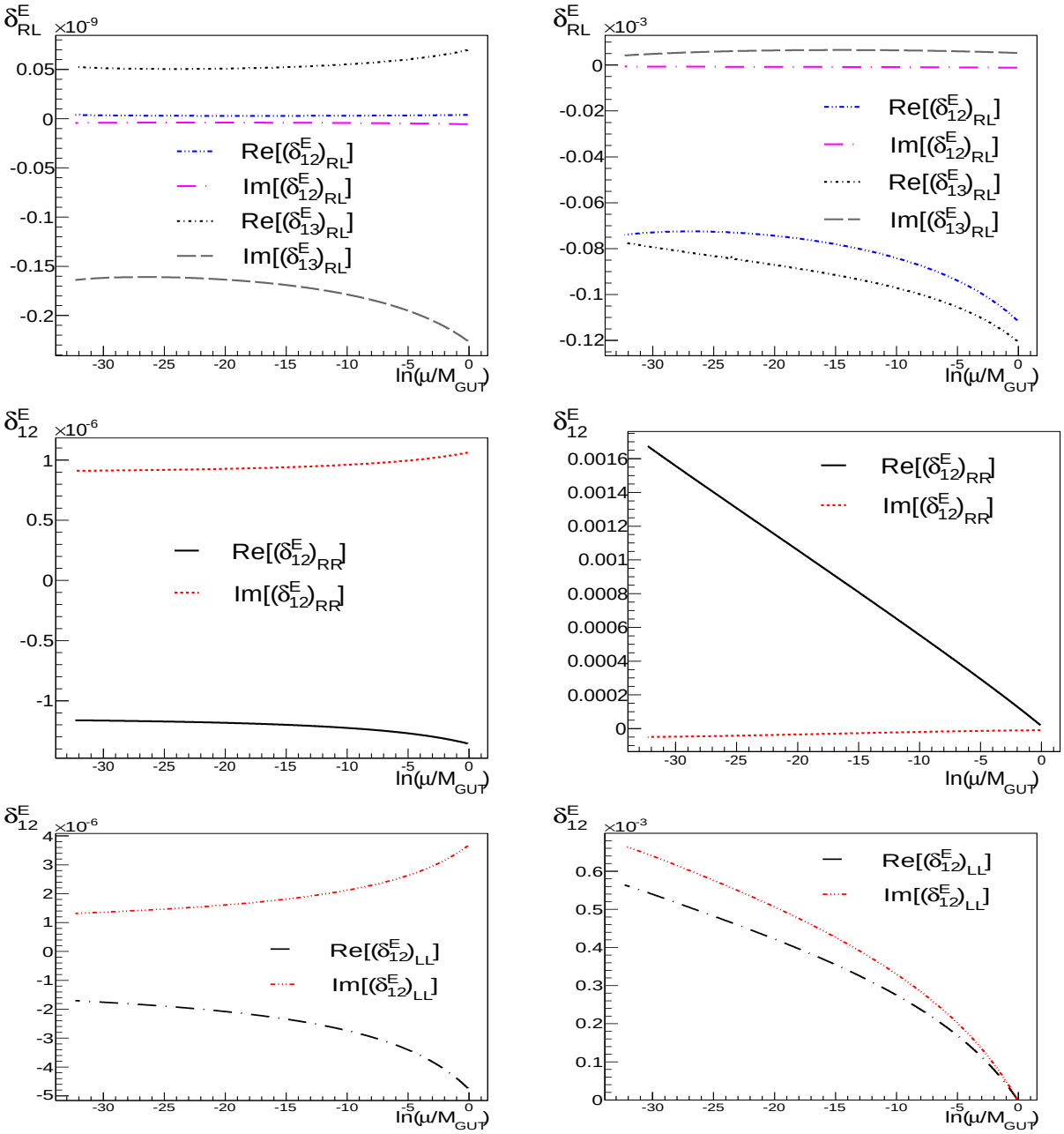

Figure 8: *Comparison of the runnings of the E-lepton flavor-violating parameters δ for A1 (left panels) and A4 (right panels), for* $(\delta^E_{1i})_{LR}$, $i = 2, 3$, *and* $(\delta^E_{12})_{XX}$, $X = L, R$.

From Table 4 we can see that this is the case for all the real parts of the flavor-violating parameters, specially for $(\delta^E_{1j})_{\{LR,RL\}}$ for $j = 2, 3$. This can again be understood in terms of the evolution of the different terms entering into the beta function of the E trilinear terms. These have the same form of Eq (37) with the replacement $D \to E$, and no analogous U terms since we are not considering neutrinos. We can see that in general all flavor-violating parameters coming entirely from the soft-squared masses (i.e., RR and LL) have a milder change than from the LR counterparts, as expected from the analogous form of the terms

entering into the m_E^2 beta function (analogous to Eq (36) with the proper replacements).

For A4, the parameter $|\mathrm{Re}[(\delta^{\mathrm{E}}_{12})_{\mathrm{LL}}]|$ exceeds the limit of the general analysis of [38], and most of the other parameters are at their limits. The different orders of magnitude of the real and imaginary parts of $(\delta^{L,E}_{ij})_{\{XY\}}$ are given in Tables 4 and 5, respectively.

	A1	A4	Bound (Process) [38]
$\mathrm{Re}[(\delta^{\mathrm{E}}_{12})_{\mathrm{RR}}]$	-1×10^{-6}	2×10^{-3}	10^{-3} $(\mu\to e\gamma)$
$\mathrm{Re}[(\delta^{\mathrm{E}}_{12})_{\mathrm{LL}}]$	-2×10^{-6}	6×10^{-4}	10^{-5} $(\mu\to e\gamma)$
$\mathrm{Re}[(\delta^{\mathrm{E}}_{12})_{\{\mathrm{LR,RL}\}}]$	4×10^{-12}	-7×10^{-5}	10^{-5} $(\mu\to e\gamma)$
$\mathrm{Re}[(\delta^{\mathrm{E}}_{21})_{\{\mathrm{LR,RL}\}}]$	2×10^{-9}	-7×10^{-5}	10^{-5} $(\mu\to e\gamma)$
$\mathrm{Re}[(\delta^{\mathrm{E}}_{13})_{\mathrm{RR}}]$	-1×10^{-5}	-5×10^{-3}	10^{-2} $(\tau\to e\gamma)$
$\mathrm{Re}[(\delta^{\mathrm{E}}_{13})_{\mathrm{LL}}]$	-2×10^{-5}	-2×10^{-3}	10^{-3} $(\tau\to e\gamma)$
$\mathrm{Re}[(\delta^{\mathrm{E}}_{13})_{\{\mathrm{LR,RL}\}}]$	5×10^{-11}	-8×10^{-5}	10^{-2} $(\tau\to e\gamma)$
$\mathrm{Re}[(\delta^{\mathrm{E}}_{31})_{\{\mathrm{LR,RL}\}}]$	3×10^{-9}	-9×10^{-5}	10^{-2} $(\tau\to e\gamma)$
$\mathrm{Re}[(\delta^{\mathrm{E}}_{23})_{\mathrm{RR}}]$	-5×10^{-4}	2×10^{-2}	10^{-2} $(\tau\to \mu\gamma)$
$\mathrm{Re}[(\delta^{\mathrm{E}}_{23})_{\mathrm{LL}}]$	-6×10^{-4}	7×10^{-3}	10^{-2} $(\tau\to \mu\gamma)$
$\mathrm{Re}[(\delta^{\mathrm{E}}_{23})_{\{\mathrm{LR,RL}\}}]$	0	5×10^{-4}	10^{-2} $(\tau\to \mu\gamma)$
$\mathrm{Re}[(\delta^{\mathrm{E}}_{32})_{\{\mathrm{LR,RL}\}}]$	0	5×10^{-4}	10^{-2} $(\tau\to \mu\gamma)$

Table 4: *Comparison of the real parts of the leptonic parameters $(\delta^E_{ij})_{\{XY\}}$ in Ansätze A1 and A4.*

In Fig 8 we compare the runnings of the E-lepton flavor-violating parameters δ for A1 (left panels) and A4 (right panels), for $(\delta^E_{1i})_{LR}$, $i=2,3$, and $(\delta^E_{12})_{XX}$, $X=L,R$. Although the transformation to the SCKM basis, where flavor-violating parameters are computed, has the effect of canceling partially the effect of the running of soft-squared masses, it is not enough to suppress sufficiently $\mathrm{BR}(\mu\to e\gamma)$, and in fact there is a significant increase in $\mathrm{BR}(\tau\to e\gamma)$ and $\mathrm{BR}(\tau\to \mu\gamma)$ with respect to Ansatz A1, see Tables 6-7.

In addition, from the imaginary parts of $|\mathrm{Im}[(\delta^{\mathrm{D,E}}_{\mathrm{ij}})_{\mathrm{XY}}]|$ we can get a significant contribution to the EDMs [40]. We have used the `SUSY_FLAVOR` code [34] to compute the EDMs, but we can understand easily how the imaginary parts of the flavor-violating parameters are constrained. The constrained combinations are

$$\delta^f_{131}\equiv \mathrm{Arg}\left[(\delta^{\mathrm{f}}_{13})_{\mathrm{LL}}(\delta^{\mathrm{f}}_{33})_{\mathrm{LR}}(\delta^{\mathrm{f}}_{31})_{\mathrm{RR}}\right],\quad \mathrm{f}=\mathrm{D},\mathrm{E}. \tag{23}$$

Since A1 and A2 differ in their D sectors, a direct difference in the values of the neutron EDM is expected (as reflected in Table 6). Note that, in Fig. 9, both the real and imaginary parts of $(\delta^f_{13})_{LL}$ and $(\delta^f_{13})_{RR}$ become important. Specifically, the leading term of the imaginary part of $(\delta^f_{13})_{LL}(\delta^f_{33})_{LR}(\delta^f_{31})_{RR}$ is

$$\mathrm{Im}[(\delta^{\mathrm{f}}_{13})_{\mathrm{LL}}]\mathrm{Re}[(\delta^{\mathrm{f}}_{33})_{\mathrm{LR}}]\mathrm{Re}[(\delta^{\mathrm{f}}_{31})_{\mathrm{RR}}]+\mathrm{Re}[(\delta^{\mathrm{f}}_{13})_{\mathrm{LL}}]\mathrm{Re}[(\delta^{\mathrm{f}}_{33})_{\mathrm{LR}}]\mathrm{Im}[(\delta^{\mathrm{f}}_{31})_{\mathrm{RR}}].$$

In [40] sensitivities for the quantities δ^f_{131} defined in Eq (23) were computed using the mass insertion approximation with a common scale for soft masses of 1 TeV. It was found, in particular, that $\delta^f_{131}\sim 10^{-4}-10^{-3}$. Since our model has specific and correlated values for the soft parameters, we can compare the impacts of $(\delta^f_{13})_{LL}$ and $(\delta^f_{13})_{RR}$ directly to the neutron EDM. We note that the imaginary parts of $(\delta^f_{13})_{LL}$ and $(\delta^f_{13})_{RR}$ in A2 found in Table 3 are approximately one order of magnitude smaller than the corresponding parameters in A1. Hence the neutron EDM is slightly decreased (by less than an order of magnitude), as seen in Table 6. Using these results, in Section 4 we place bounds on $(\delta^f_{13})_{LL}$ and $(\delta^f_{13})_{RR}$ by saturating the EDM bound.

	A1	A4
$\mathrm{Im}[(\delta^{\mathrm{E}}_{12})_{\mathrm{RR}}]$	9×10^{-7}	-5×10^{-5}
$\mathrm{Im}[(\delta^{\mathrm{E}}_{12})_{\mathrm{LL}}]$	1×10^{-6}	7×10^{-4}
$\mathrm{Im}[(\delta^{\mathrm{E}}_{12})_{\{\mathrm{LR,RL}\}}]$	-4×10^{-12}	-6×10^{-7}
$\mathrm{Im}[(\delta^{\mathrm{E}}_{21})_{\{\mathrm{LR,RL}\}}]$	2×10^{-9}	-6×10^{-6}
$\mathrm{Im}[(\delta^{\mathrm{E}}_{13})_{\mathrm{RR}}]$	4×10^{-5}	4×10^{-4}
$\mathrm{Im}[(\delta^{\mathrm{E}}_{13})_{\mathrm{LL}}]$	-5×10^{-4}	-3×10^{-3}
$\mathrm{Im}[(\delta^{\mathrm{E}}_{13})_{\{\mathrm{LR,RL}\}}]$	-2×10^{-10}	4×10^{-6}
$\mathrm{Im}[(\delta^{\mathrm{E}}_{31})_{\{\mathrm{LR,RL}\}}]$	3×10^{-5}	2×10^{-4}
$\mathrm{Im}[(\delta^{\mathrm{E}}_{23})_{\mathrm{RR}}]$	5×10^{-6}	6×10^{-5}
$\mathrm{Im}[(\delta^{\mathrm{E}}_{23})_{\mathrm{LL}}]$	6×10^{-6}	-8×10^{-4}
$\mathrm{Im}[(\delta^{\mathrm{E}}_{23})_{\{\mathrm{LR,RL}\}}]$	0	9×10^{-7}
$\mathrm{Im}[(\delta^{\mathrm{E}}_{23})_{\{\mathrm{LR,RL}\}}]$	0	4×10^{-5}

Table 5: *Comparison of the imaginary parts of the leptonic parameters $(\delta^f_{ij})_{\{XY\}}$ in Ansätze A1 and A4.*

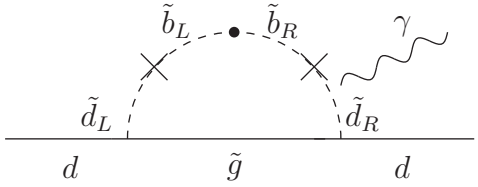

Figure 9: *Contribution of flavor-violating process to the d-quark EDM.*

3.4 Comments on the results and comparison to observables

Ansätze A1 and A2 predict acceptable flavor violation, while Ansätze A3 and A4 do not. We recall that the properties of the D and L sectors are controlled by the $\bar{\mathbf{5}}$ sector of $SU(5)$, whereas the Q, U and E sectors are controlled by the **10** sector. The premise of the Ansatz A4 for the Yukawa couplings, Eq (18), was that if soft mass-squared sectors were transformed to the SCKM basis by the same transformations as the corresponding Yukawa sectors, then the off-diagonal parameters of the corresponding sectors would be suppressed because the off-diagonal elements of m^2_f would be mainly rotated away with the same matrices that make the Yukawa couplings diagonal. This is largely the case for the D sector: in the cases of $(m^2_f)_{13}$ and $(m^2_f)_{23}$, for $f = D$, the rotation to the SCKM matrix produces a smaller matrix element than in the non-SCKM basis. However, this is not the case for other sectors, where too much flavor violation is produced. On the other hand, in the cases of Ansätze A2 and A1, the rotation to the SCKM basis effectively rotates away any large flavor violation.

For A1, with the E_{LL} sector we expected a similar behavior (because the sector is directly linked to the diagonalizing matrices of h_E), but the rotation away of parameters is not as successful as in the D sector (see Fig. 8). For the sectors Q, U and E, associated with the 10 sector of $SU(5)$, which is treated as having diagonal matrices, the off-diagonal elements of m^2_f for $f = Q,\ D,\ U$ appear as a consequence of the off-diagonal elements of m^2_f for $f = E, L$. So they are not related, in principle, but since the Yukawa couplings h_d and h_e are related, we expected that the SCKM transformations of the soft sectors Q and E would

tend also to suppress the off diagonal elements. This is however not the case for them, specially for the E sector, where the off-diagonal elements may be considerably enlarged, as seen in Fig. 8.

In Tables 6 and 7 we compare the values of the relevant observables predicted by the Ansätze Eq (15)-Eq (18), and the corresponding current experimental values.

The CP-violating parameter ϵ' could give important constraints on models where LR flavor-violating contributions are much bigger than their RR and LL counterparts: $|(\delta^D_{ij})_{RL}| \gg |(\delta^D_{ij})_{XX}|$, $X = R, L$. This is not the case in our framework, where both the real and imaginary parts of $[(\delta^D_{ij})_{XX}]$ are much bigger than $[(\delta^D_{ij})_{RL}]$. Furthermore, chirality-conserving mass insertion parameters turn out to be more stringently constrained from Δm_K and ϵ_K [46], which enter as combinations of the real and imaginary parts of $(\delta^D_{ij})_{XX}$ for the combinations $ij = \{12, 21\}$ [47]. However, regarding Δm_K, even in the Standard Model precise computations are not possible due to unknown long-distance contributions. Hence, we compare the best estimate obtained from the short-distance (SD) contributions [48], denoted by $\Delta m_K^{SD} = (3.1 \pm 1.2) \times 10^{-15}$, to the experimental value, see Table 7. We see that the central value of Δm_K^{SD} accounts for 86% of the experimental central value, and its uncertainty can easily account for the reported experimental value within 1σ. The value that we obtain in our model also lies comfortably within 1σ of the experimental value, taking into account the SD uncertainty. For Δm_{B_s}, the SM value is $(17.70 \pm 15\%)$, and the value that we obtain is in better agreement with the experimental value.

4 Beyond No-Scale GUTs: Maximal Flavour Violation

In this Section we explore the possibilities for deformations of the pure no-scale boundary conditions with non-vanishing scalar masses. We study the conditions under which flavour violation could be maximal, in the sense that off-diagonal entries in the scalar mass matrices could be as large as the diagonal entries at some super-GUT input scale $M_{in} > M_{\rm GUT}$. We emphasize that, as in the previous Section, we are not trying to explain any observed effects, but rather to set limits on the sizes of the possible off-diagonal terms using current measurements. When these are as large as the diagonal terms, we are in the regime we have called MaxSFV.

This analysis builds upon that in the previous Sections, in which we analysed the most powerful flavour constraints in representative no-scale SU(5) GUT scenarios. To this end, we consider scalar mass-squared matrices with universal flavour-diagonal entries and consider the effects of switching real off-diagonal real entries on, one at a time. There are in fact far too many possible parameter combinations in general. Thus, in order to see the effect of the additional (off-diagonal) parameters and to be concrete, we make some simplifying assumptions and test these one by one (in terms of generations).

Thus we consider matrices of the form

$$m^2_{\bar{5}} = \begin{pmatrix} a & b & 0 \\ b & a & 0 \\ 0 & 0 & a \end{pmatrix}, \quad m^2_{\bar{5}} = \begin{pmatrix} a & 0 & b \\ 0 & a & 0 \\ b & 0 & a \end{pmatrix}, \quad m^2_{\bar{5}} = \begin{pmatrix} a & 0 & 0 \\ 0 & a & b \\ 0 & b & a \end{pmatrix}, \tag{24}$$

Relevant observables for A1 and A2			
	Experimental Values		
EDMs [e cm]		A1	A2
Electron EDM	$< 8.7 \times 10^{-29}$[23]	1.11×10^{-30}	1.19×10^{-30}
Muon EDM	$-(0.1 \pm 0.9) \times 10^{-19}$[23]	3.49×10^{-30}	3.63×10^{-30}
Tau EDM	-1.27×10^{-25}	6.92×10^{-30}	7.13×10^{-30}
Neutron EDM	$< 2.9 \times 10^{-26}$[23] $O(10^{-28})$[41]	-1.17×10^{-28}	-7.18×10^{-29}
M. Anomalies			
Δa_e	8.2×10^{-13}[42]	1.43×10^{-14}	1.43×10^{-14}
Δa_μ	$(2.87 \pm 0.80) \times 10^{-8}$	6.15×10^{-10}	6.16×10^{-10}
Δa_τ	$(-5.3 \times 10^{-2}, 1.2 \times 10^{-3})$	1.80×10^{-7}	1.80×10^{-7}
$l^j \to l^i \gamma$ decays			
BR($\mu \to e\gamma$)	$< 5.7 \times 10^{-13}$ [43]	5.3×10^{-16}	5.4×10^{-16}
BR($\tau \to e\gamma$)	$< 3.3 \times 10^{-8}$ [44]	1.2×10^{-13}	1.2×10^{-13}
BR($\tau \to \mu\gamma$)	$< 4.4 \times 10^{-8}$ [44]	6.0×10^{-12}	6.2×10^{-12}
B decays			
BR($B_s \to \mu^+\mu^-$)	$(2.9 \pm 0.7 \times 10^{-9})$ [35]	3.4×10^{-9}	3.4×10^{-9}
Untagged		3.75×10^{-9}	3.76×10^{-9}
BR($B_d \to \mu^+\mu^-$)	$(3.6^{+1.6}_{-1.4})10^{-10}$ [35]	1.1×10^{-10}	1.0×10^{-10}
BR($B_s \to \mu^+e^-$)	$< 2.0 \times 10^{-7}$	2.09×10^{-27}	2.13×10^{-27}
BR($B \to \tau\nu$)	$(1.20 \pm 0.25) \times 10^{-4}$	7.43×10^{-5}	7.43×10^{-5}
BR($B \to X_s\gamma$)	$(3.55 \pm 0.24 \pm 0.09) \times 10^{-4}$ [45]	3.92×10^{-4}	3.92×10^{-4}
ν Kaon decays			
BR($K_L^0 \to \pi^0\nu\nu$)	$< 2.6 \times 10^{-8}$	2.32×10^{-11}	2.32×10^{-11}
BR($K^+ \to \pi^+\nu\nu$)	$(1.7 \pm 1.1) \times 10^{-10}$	7.64×10^{-11}	7.64×10^{-11}
KK mixing			
$\lvert\epsilon_K\rvert$	$(2.223 \pm 0.010)10^{-3}$	1.81×10^{-3}	1.81×10^{-3}
Δm_K [GeV]	$(3.63 \pm 0.0059) \times 10^{-15}$	2.63×10^{-15}	2.63×10^{-15}
BB mixings			
Δm_{B_d}	$(3.36 \pm 1.97 \times 10^{-2}) \times 10^{-13}$	3.05×10^{-13}	
Δm_{B_s}	$(1.164 \pm 1.4 \times 10^{-3}) \times 10^{-11}$	0.98×10^{-11}	

Table 6: *Comparison of the predictions for Ansätze A1 and A2 with the experimental values. The values have been obtained with the* `SUSY_FLAVOR` *code. Without flavor violation, we obtain* $BR(B \to X_s\gamma) = 4.01 \times 10^{-4}$. *The value in the Table, which includes flavor violation, is consistent with experiment within* 2σ, *taking into account the Standard Model uncertainty of* 0.23×10^{-4}. *The NNLO Standard Model value of* $|\epsilon_K|$ *is* $(1.81 \pm 0.28) \times 10^{-3}$. *See Section 3.4 for notes regarding the values of* Δm_K *and* Δm_{B_s} .

Relevant observables for A3 and A4			
	Experimental Values		
EDMs [e cm]		A3	A4
Electron EDM	$< 8.7 \times 10^{-29}$[23]	6.42×10^{-28}	2.7×10^{-27}
Muon EDM	$-(0.1 \pm 0.9) \times 10^{-19}$[23]	-1.40×10^{-28}	-3.0×10^{-27}
Tau EDM	-1.27×10^{-25}	4.57×10^{-28}	3.7×10^{-28}
Neutron EDM	$< 2.9 \times 10^{-26}$[23] $O(10^{-28})$[41]	-3.59×10^{-29}	3.7×10^{-30}
M. Anomalies			
Δa_e	8.2×10^{-13}[42]	3.2×10^{-14}	1.2×10^{-14}
Δa_μ	$(2.87 \pm 0.80) \times 10^{-8}$	1.4×10^{-9}	6.1×10^{-10}
Δa_τ	$(-5.3 \times 10^{-2}, 1.2 \times 10^{-3})$	4.1×10^{-7}	1.8×10^{-7}
$l^j \to l^i \gamma$ decays			
BR($\mu \to e\gamma$)	$< 5.7 \times 10^{-13}$ [43]	1.7×10^{-9}	7.49×10^{-10}
BR($\tau \to e\gamma$)	$< 3.3 \times 10^{-8}$ [44]	6.6×10^{-13}	1.02×10^{-12}
BR($\tau \to \mu\gamma$)	$< 4.4 \times 10^{-8}$ [44]	1.05×10^{-11}	1.52×10^{-12}
B decays			
BR($B_s \to \mu^+\mu^-$)	$(2.9 \pm 0.7 \times 10^{-9})$ [35]	3.3×10^{-9}	3.4×10^{-9}
Untagged		3.66×10^{-9}	3.75×10^{-9}
BR($B_d \to \mu^+\mu^-$)	$(3.6^{+1.6}_{-1.4})10^{-10}$ [35]	1.4×10^{-10}	1.1×10^{-10}
BR($B_s \to \mu^+e^-$)	$< 2.0 \times 10^{-7}$	9.1×10^{-23}	2.3×10^{-21}
BR($B \to \tau\nu$)	$(1.20 \pm 0.25) \times 10^{-4}$	7.37×10^{-5}	7.43×10^{-5}
BR($B \to X_s\gamma$)	$(3.55 \pm 0.24 \pm 0.09) \times 10^{-4}$ [45]	4.22×10^{-4}	3.9×10^{-4}
ν Kaon decays			
BR($K_L^0 \to \pi^0\nu\nu$)	$< 2.6 \times 10^{-8}$	2.32×10^{-11}	2.3×10^{-11}
BR($K^+ \to \pi^+\nu\nu$)	$(1.7 \pm 1.1) \times 10^{-10}$	7.6×10^{-11}	7.6×10^{-11}
KK mixing			
$\lvert\epsilon_K\rvert$	$(2.223 \pm 0.010)10^{-3}$	1.82×10^{-3}	1.81×10^{-3}
Δm_K [GeV]	$(3.483 \pm 0.0059) \times 10^{-15}$	2.63×10^{-15}	2.63×10^{-15}

Table 7: *Comparison of the predictions for our Ansätze A3 and A4 with the experimental values.*

and

$$m_{10}^2 = \begin{pmatrix} c & d & 0 \\ d & c & 0 \\ 0 & 0 & c \end{pmatrix}, \quad m_{10}^2 = \begin{pmatrix} c & 0 & d \\ 0 & c & 0 \\ d & 0 & c \end{pmatrix}, \quad m_{10}^2 = \begin{pmatrix} c & 0 & 0 \\ 0 & c & d \\ 0 & d & c \end{pmatrix}, \tag{25}$$

for $a \neq b$ and $c \neq d$, with all four parameters real. The rest of the boundary conditions at M_{in} are taken to be the same as in Sec 2.2. We start by considering separately the boundary conditions (24) and (25), treating each sector separately.

4.1 Off-diagonal entries in $\mathbf{m}_{\bar{\mathbf{5}}}^2$ and $\mathbf{m}_{\mathbf{10}}^2$

4.1.1 The $(1,2)$ sector

The inputs (24) imply the following universal matching conditions at $M_{\rm GUT}$:

$$m_{D_{12}}^2 = m_{L_{12}}^2 = m_{\bar{5}_{12}}^2 \,, \tag{26}$$

which will have the strongest impact on observables where $m_{D_{12}}^2$, $m_{L_{12}}^2$ enter at one loop level. In the lepton sector, this is the case for the amplitude of the process $\mu \to e\gamma$, shown in Fig. 10. This amplitude can be written as $\mathcal{M}_{\mu e\gamma} = \frac{e}{2m_\mu}\, \epsilon^{*\alpha} \bar{u}_e(k+q)\, [i\sigma_{\beta\alpha} q^\beta (a_{\mu e\gamma R} P_L + a_{\mu e\gamma L} P_R)]\, u_\mu(k)$ where $\sigma_{\alpha\beta} = i/2\, [\gamma_\alpha, \gamma_\beta]$, ϵ^α is the photon polarization vector, k and $k+q$ are on-shell momenta, u_μ, $\bar{u}_\mu$ are spinors that satisfy the Dirac equation and $P_{R,L} = (1 \pm \gamma_5)/2$. The L/R index in $a_{\mu e\gamma L/R}$ refers to the electron chirality. In terms of $a_{\mu e\gamma L}$ and $a_{\mu e\gamma R}$, we have

$$\mathrm{BR}(\mu \to e\gamma) = \frac{3\pi^2 e^2}{G_F^2 m_\mu^4} \left(|a_{\mu e\gamma L}|^2 + |a_{\mu e\gamma R}|^2\right). \tag{27}$$

In fact, if $\tan\beta$ is large and $\mu > M_2 > M_1$, the dominant contribution to $\mathrm{BR}(\mu \to e\gamma)$ is mediated by bino exchange, which is represented in the flavor basis by the mass-insertion diagrams of the second row in Fig. 10. The contributions to $a_{\mu e\gamma L,R}$ in the mass eigenstate basis are schematically as follows [49]

$$\begin{aligned} a_{\mu e\gamma L} &\approx g_1^2 \frac{m_\mu}{48\pi^2} \sum_m K_{m1}^* K_{m5} \frac{M_1}{m_{L_m}^2} F_2^N \left(\frac{m_{\tilde{\chi}_1^0}^2}{m_{L_m}^2}\right), \\ a_{\mu e\gamma R} &\approx g_1^2 \frac{m_\mu}{48\pi^2} \sum_m K_{m4}^* K_{m2} \frac{M_1}{m_{L_m}^2} F_2^N \left(\frac{m_{\tilde{\chi}_1^0}^2}{m_{L_m}^2}\right), \end{aligned} \tag{28}$$

where the matrices K diagonalize the squared-mass matrices, Eq (34). The mass eigenstate index 1 in $K_{m1}^* K_{m5}$, corresponds roughly to $\tilde{e}_L$ while the index 5 to $\tilde{\mu}_L$. Analogously in $K_{m4}^* K_{m2}$, the index 4 roughly corresponds to $\tilde{\mu}_R$, while the index 2 refers to $\tilde{e}_R$, and F_2^N denotes the loop function involved in each diagram. All other contributions involve higgsinos and are therefore suppressed for large μ. We note that in Eqs. (28), all indices $m = 1, 2, \ldots, 6$ give contributions to $\mathrm{BR}(\mu \to e\gamma)$. When $\hat{m}_{E(RR)_{12}}^2$ is significantly suppressed with respect to $\hat{m}_{E(LL)_{12}}^2$, which is our case since the seed for $\hat{m}_{E(RR)}^2$ is m_{10}^2, whereas the seed for $\hat{m}_{E(LL)}^2$ is m_5^2, then $a_{\mu e\gamma L}$ dominates. Its main contributions come from mass eigenstates mainly containing $\tilde{e}_L$, $\tilde{\mu}_L$ and $\tilde{\mu}_R$, provided that flavor-violating LR parameters are smaller than LL and RR, which is also our case. Then the most important contributions in $a_{\mu e\gamma L}$ come when $\tilde{\ell}_m = \tilde{e}_L$, $\tilde{\mu}_L$ and $\tilde{\mu}_R$, and for each of them

$$K_{m1}^* K_{m5} \approx t_{\tilde{l}_m} (\delta_{22}^E)_{LR} (\delta_{12}^E)_{LL} \big|_{\tilde{\ell}_m \approx \tilde{e}_L, \tilde{\mu}_L, \tilde{\mu}_R} \,, \tag{29}$$

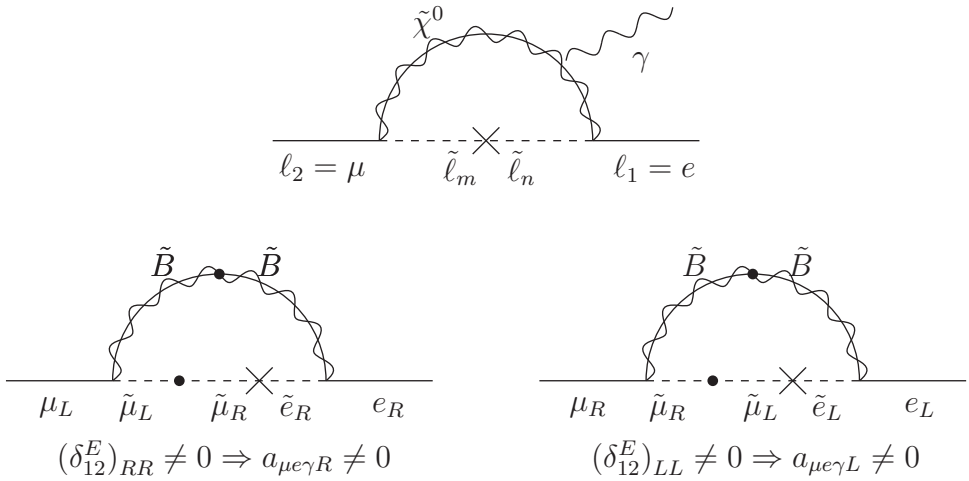

Figure 10: *Top: Loop diagram representing the transition $\ell_2 \to \ell_1\gamma$ in mass eigenstates, with ℓ_i being the lepton mass eigenstates, in our Ansatz 1 $\ell_2 = \mu$ and $\ell_1 = e$, and $\tilde{\ell}_m$ the sleptons eigenstates, $m = 1, 2, \ldots, 6$. Bottom: Leading contributions to $a_{\mu e\gamma}$ in the case of large μ, represented in the flavor basis.*

where $t_{\tilde{l}_m}$ is a number of $O(1)$ and is different for each of the terms above [49]. Hence, once $m^2_{\bar{5}_{12}}$ is non-zero at the input scale, the parameter $m^2_{L_{12}}$ is significantly bigger at the GUT scale than in the no-scale supergravity case, and this directly impacts the increase of $a_{\mu e\gamma L}$ and hence BR($\mu \to e\gamma$). In the quark sector, the analogous increase of $m^2_{D_{12}}$ at the GUT scale will have an impact in the analogous amplitude to $a_{\mu e\gamma R}$, that is $a_{sd\gamma R}$, but this time the Standard Model contribution to the decay $s \to d\gamma$ will be the dominant one, with supersymmetry making only a tiny correction [50]. We observe that $m^2_{D_{12}}$ affects the observable BR($B_d \to \mu^+\mu^-$) because it enters through a penguin diagram with Higgsinos and sleptons in the loop, but also in this case the contribution is tiny in comparison to the SM contribution [51]. Finally, Δm_K and hence ϵ_K are affected by $m^2_{D_{12}}$ but in this case the contributions coming from the small flavor-violating parameters in Ansatz 1 do not have an effect, as these parameters should typically be of $O(10^{-2})$ to have an impact in changing the values of ϵ_K and Δm_K [47].

We plot in Fig 11 the value of BR($\mu \to e\gamma$) as a function of $b = m^2_{\bar{5}_{12}}$, for the three choices $a = m^2_{\bar{5}_{ii}} = 0$, 6×10^4 GeV^2 and 1.4×10^5 GeV^2. In the first panel we take $m^2_{10_{ii}} = 0$ ($c = d = 0$), whereas in the second panel $m^2_{10_{ii}} = m^2_{\bar{5}_{ii}}$ ($c = a$, $d = 0$). The results are quite similar, though there are differences in the supersymmetric spectra. In both cases we find that BR($\mu \to e\gamma$) requires $m^2_{\bar{5}_{12}} = b \lesssim 170$ GeV^2 for small $m^2_{\bar{5}_{ii}} = a \to 0$. This means that flavour violation among the scalar masses-squared in the $(1, 2)$ sector could be maximal, i.e., $b/a \sim 1$, if the universal diagonal entry $m^2_{\bar{5}_{ii}} = a \lesssim 170$ GeV^2. As one would expect, larger values of $m^2_{\bar{5}_{12}}$ would be allowed for larger values of $m^2_{\bar{5}_{ii}}$, but the ratio b/a could not reach unity. We consider the choice $m^2_{\bar{5}_{ii}} = 1.4 \times 10^5$ GeV^2 as an upper limit for a since, for higher values, the spectrum is sufficiently different from our original benchmark **B** that it no longer satisfies the constraint on the relic density. In this case, the upper limit on b is 210 (220) GeV^2 for $m^2_{10_{ii}} = 0$ ($= a$), so we must require $b \ll a$. In the third panel of Fig 11 we consider the effects of the off-diagonal components in m^2_{10}. Here, we have set $m^2_{10_{ii}} = m^2_{\bar{5}_{ii}}$ with $m^2_{\bar{5}_{12}} = 0$ ($c = a$, $b = 0$), and have plotted the branching ratio as a function of $d = m^2_{10_{12}}$. As one can see, the constraint on d is much weaker than the analogous constraint on b.

We conclude that the MaxSFV scenario is possible in the (1, 2) sector if $m^2_{\bar{5}_{12}} = b \lesssim 170$ GeV^2, and if $m^2_{10_{12}} = d \lesssim 520$ GeV^2 as summarized in Table 8.

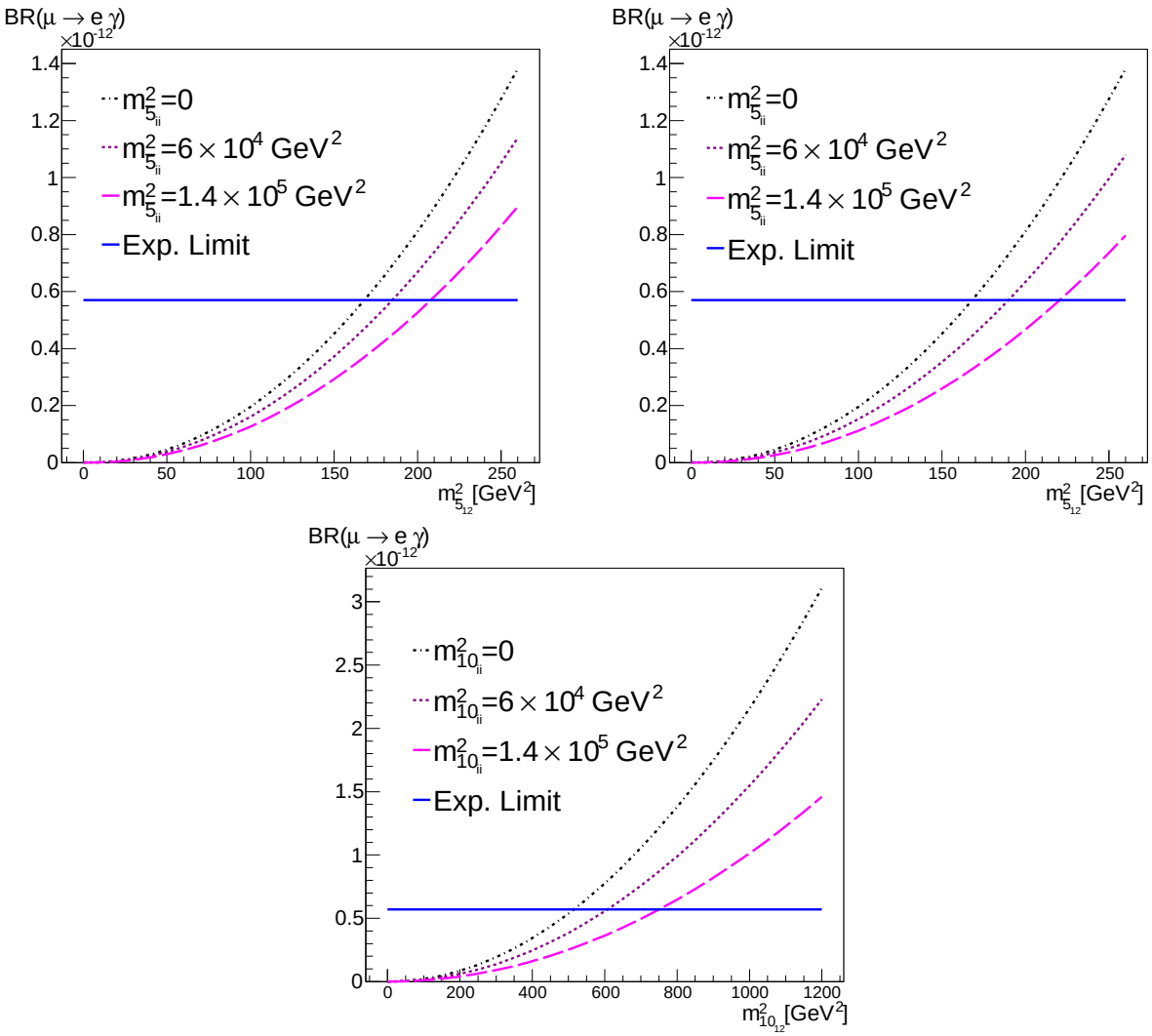

Figure 11: *Top:* $b = m^2_{\bar{5}_{12}}$ *vs.* $BR(\mu \to e\gamma)$ *for* $a = m^2_{\bar{5}_{ii}} = 0,\ 6\times10^4\ GeV^2$ *and* $1.4\times10^5\ GeV^2$. *In the first panel,* $m^2_{10} = 0$ $(c = d = 0)$, *while in the second* $m^2_{10_{ii}} = m^2_{\bar{5}_{ii}}$ $(c = a,\ d = 0)$. *Bottom:* $d = m^2_{10_{12}}$ *vs.* $BR(\mu \to e\gamma)$, *where only off-diagonal elements of* m^2_{10} *were set using* $m^2_{10_{ii}} = m^2_{\bar{5}_{ii}}$ *(that is* $c = a,\ b = 0$*).*

4.1.2 The $(1,3)$ sector

We see from Eq. 31 that, once the Yukawa couplings are complex, then the soft-squared masses and trilinear terms also become complex. We remind the reader that the only source of CP violation stems from the CKM phase, which through Eq (15) translates into the complex Yukawa couplings, Eq (14). Then, once an imaginary seed for $m^2_{\bar{5}_{13}}$ is set, a real non-zero entry at M_{in} for $m^2_{\bar{5}_{13}}$ will increase faster for both the imaginary and real parts of $m^2_{\bar{5}_{13}}$, than in the case of the pure no-scale set up.

We see from Table 6 that in A1 the value of the electron EDM, d_e, is already close to the experimental limit and from the diagram in Fig 9 we see the potential importance for this observable when increasing the real part of $m^2_{\bar{5}_{13}}$. In A1, the leading contribution to d_e comes from the terms in Eq (24) and once $\mathrm{Re}\left[\mathrm{m}^2_{\bar{5}_{13}}\right]$ is non-zero at M_{in}, then at the GUT scale it will be bigger than in the no-scale case and particularly $\mathrm{Re}\left[(\delta^{\mathrm{D}}_{31})_{\mathrm{RR}}\right]$ will have a significant increase. As a consequence, for $\mathrm{Re}\left[\mathrm{m}^2_{\bar{5}_{13}}\right] \neq 0$ at the input scale, the most

constraining observable is the electron EDM. Fig 12 shows d_e as a function of $b = m^2_{\bar{5}_{13}}$. The bounds on the electron EDM are shown by the two horizontal solid lines straddling $d_e = 0$. As one can see, the flavour off-diagonal entry in the squark mass matrix is bounded by $b < 10^4$ GeV^2 for our maximal value of a. Once again, allowing $c = a$ (with $d = 0$) does not greatly affect this limit. On the other hand, when we consider the EDM as a function of $d = m^2_{10_{13}}$ (with $b = 0$), we find that $d < 2000$ GeV^2 for the maximal value of $c = a$.

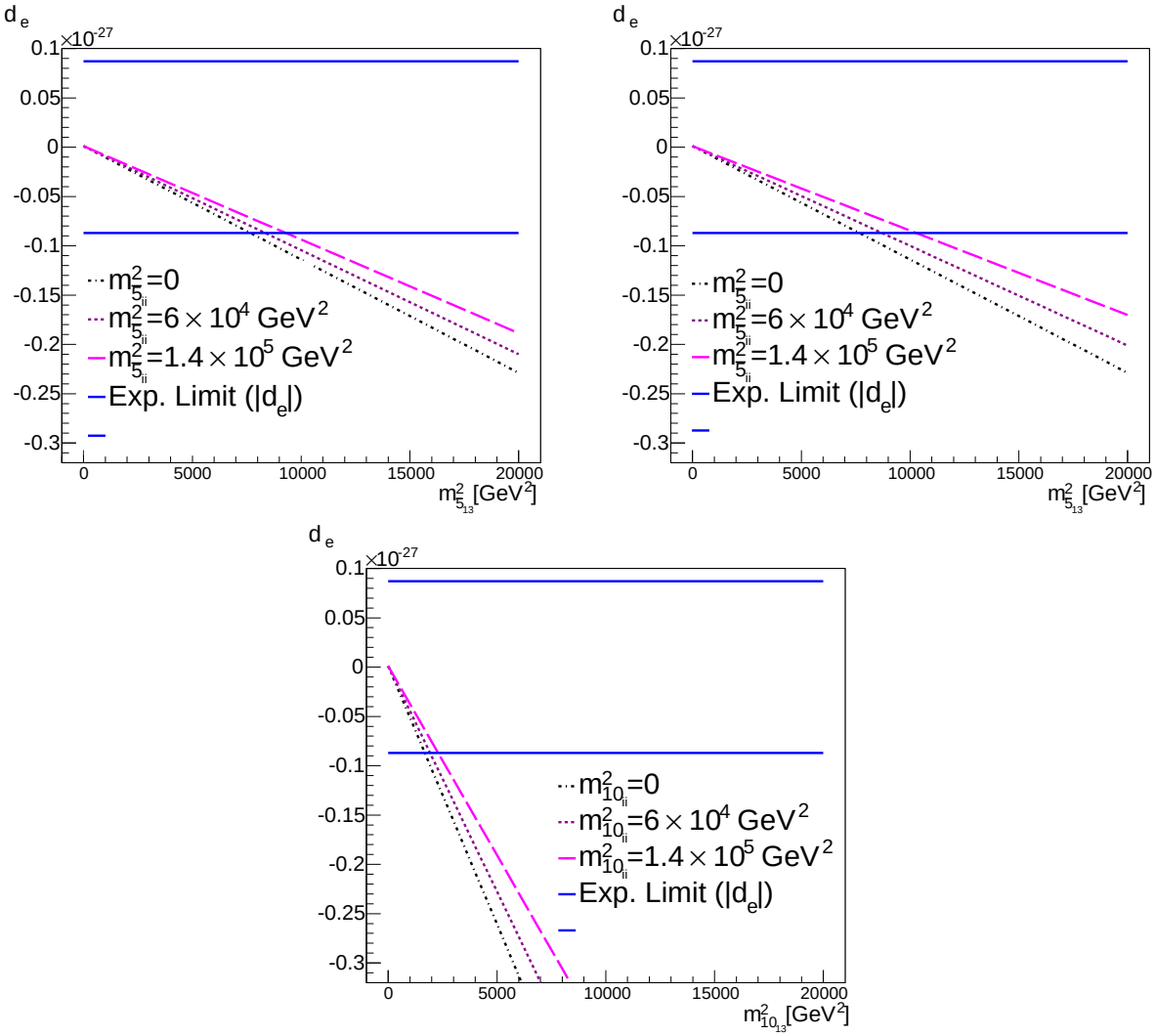

Figure 12: *Top: we show* $b = m^2_{\bar{5}_{13}}$ *vs.* d_e *for* $a = m^2_{\bar{5}_{ii}} = 0,\ 6 \times 10^5\ GeV^2$ *and* $1.4 \times 10^5\ GeV^2$*; in the first panel* $m^2_{10} = 0$ *(*$c = d = 0$*), while in the second panel* $m^2_{10_{ii}} = m^2_{5_{ii}}$ *(*$c = a,\ d = 0$*). Bottom: here we show* $d = m^2_{10_{13}}$ *vs.* d_e *for* $m^2_{\bar{5}_{ii}} = m^2_{10_{ii}}$ *(*$c = a,\ b = 0$*).*

The neutron EDM is well below the present experimental limit, but at close to the future sensitivity of $O(10^{-28})$ e-cm [41]. In Fig. 13 we show the neutron EDM as a function of $m^2_{\bar{5}_{13}}$ for three values of $m^2_{\bar{5}_{ii}} = 0,\ 6 \times 10^4$ GeV^2 and 1.4×10^5 GeV^2. The left panels shows the current (lack of) constraints, while the right panels show the anticipated future constraints. In the top row, $m^2_{10} = 0$ ($c = d = 0$). In the middle row, $m^2_{10_{ii}} = m^2_{5_{ii}}$ ($c = a,\ d = 0$), and in the bottom row, we plot d_n versus $d = m^2_{10_{13}}$ with $c = a$ and $b = 0$. As one can see, there are no current constraints on either b or d for our allowed range in a and c. However, we expect that future constraints can place a limit of about $b \lesssim 230$ GeV^2 and $d \lesssim 1540$ GeV^2.

Other parameters that are affected by switching on a non-zero off-diagonal parameter are

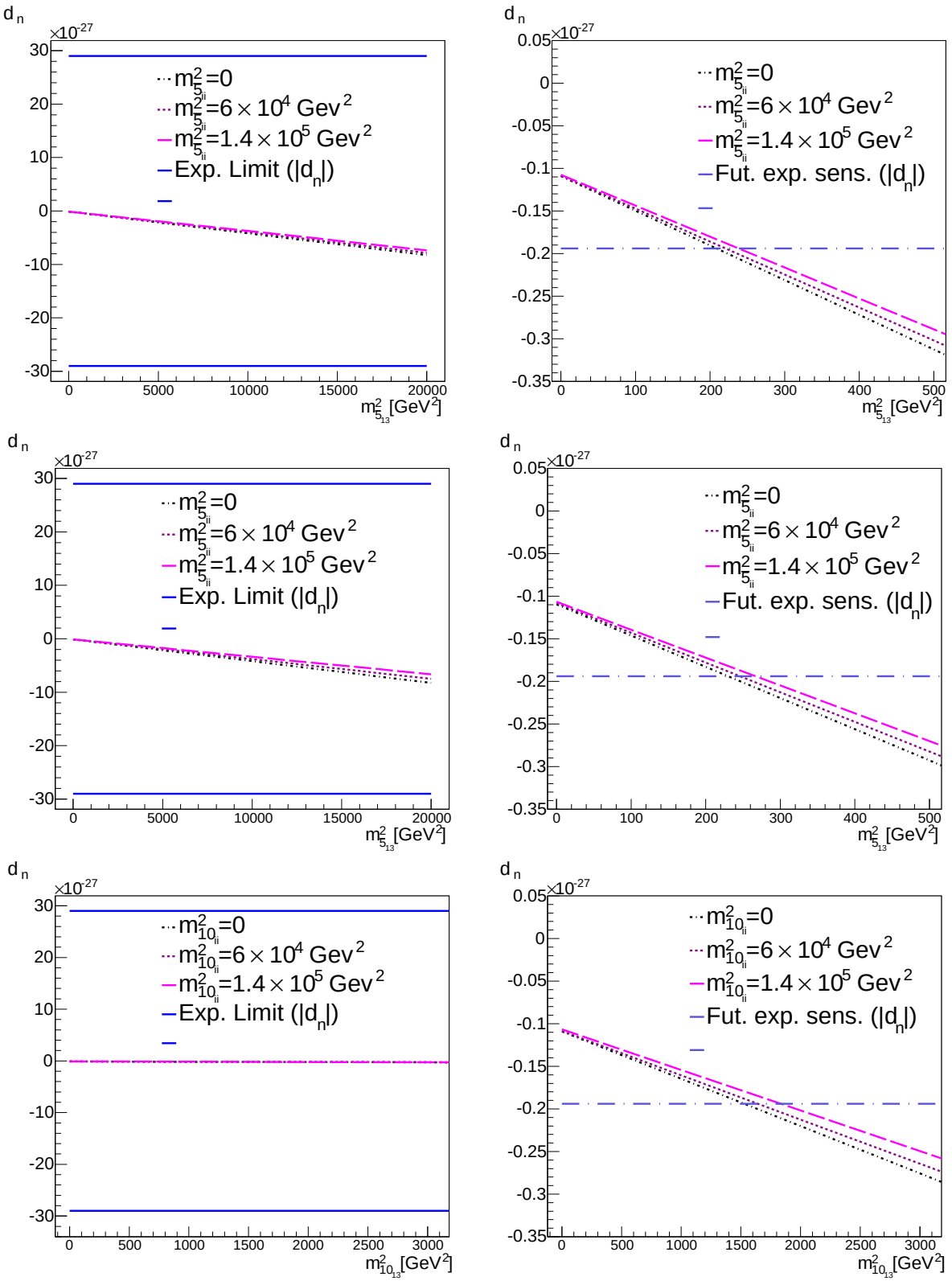

Figure 13: *Top:* $b = m^2_{\bar{5}_{13}}$ *vs.* d_n *for* $a = m^2_{\bar{5}_{ii}} = 0,\ 6\times10^5\ GeV^2$ *and* $1.4\times10^5\ GeV^2$. *Here* $m^2_{10} = 0$ $(c = d = 0)$. *For definiteness, we have used the value of* 1.94×10^{-28} *[52], for the future sensitivity. Other values (all of* $O(10^{-28})$*) can be found in [41]. Middle:* $m^2_{10_{ii}} = m^2_{\bar{5}_{ii}}$ $(c = a,\ d = 0)$. *Bottom:* $d = m^2_{10_{13}}$ *vs.* d_n *for* $m^2_{10_{ii}} = m^2_{\bar{5}_{ii}}$ $(c = a,\ b = 0)$.

ϵ_K, BR($\mu \to e\gamma$) and BR($\tau \to e\gamma$), which remain (for the most part) within the experimental limits. Fig. 14 shows the case for BR($\mu \to e\gamma$). This branching ratio is particularly sensitive to the increase in $d = m^2_{10_{13}}$ if this is allowed to grow much faster than $m^2_{10_{12}}$ and $m^2_{\bar{5}_{12}}$, which is depicted in the third panel in Fig. 14. When the real part of $m^2_{10_{13}}$ is non-zero at M_{in}, while the real parts of $m^2_{10_{12}}$ and $m^2_{\bar{5}_{12}}$ are zero, the values of $m^2_{E_{12}}$ and $m^2_{L_{12}}$ will evolve to values close to their no-scale values at $M_{\rm EW}$, producing a value for $a_{\mu e\gamma L}$ close to the no-scale case. When $m^2_{10_{13}}$ is allowed to increase to $O(10^4)$ GeV^2, the $a_{\mu e\gamma R}$ contribution to BR($\mu \to e\gamma$), will dominate over $a_{\mu e\gamma L}$, and the terms in $a_{\mu e\gamma R}$, Eq (28), for $m = 6$, which corresponds to the lightest slepton, will drive BR($\mu \to e\gamma$) to levels above the experimental bound.

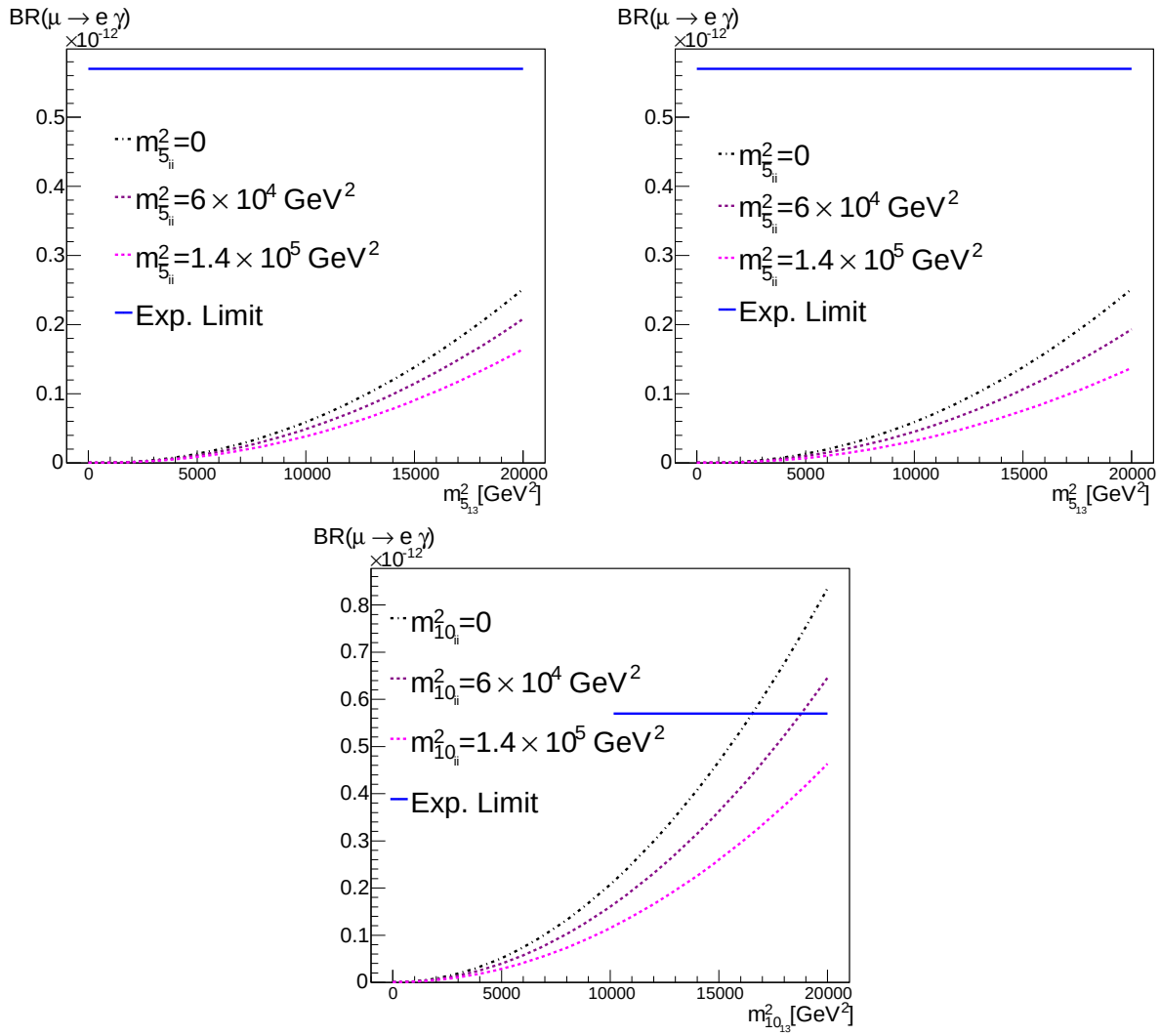

Figure 14: *Top:* $b = m^2_{\bar{5}_{13}}$ *vs.* $a = BR(\mu \to e\gamma)$ *for* $m^2_{\bar{5}_{ii}} = 0,\ 6 \times 10^4\ GeV^2$ *and* $1.4 \times 10^5\ GeV^2$. *In the first panel* $m^2_{10} = 0$ $(c = d = 0)$, *while in the second panel* $m^2_{10_{ii}} = m^2_{5_{ii}}$ $(c = a,\ d = 0)$. *Bottom:* $d = m^2_{10_{13}}$ *vs.* $BR(\mu \to e\gamma)$ *for* $m^2_{10_{ii}} = m^2_{\bar{5}_{ii}}$ $(c = a,\ b = 0)$. .

In the case of ϵ_K, the Standard Model uncertainty, which must be added to the supersymmetric value, must be taken into account. In Fig. 15 we show ϵ_K as a function of $b = m^2_{\bar{5}_{13}}$ together with the area allowed by the NNLO SM error [48] and the 2 σ experimental region. This clarifies that the value that we obtain for ϵ_K is in agreement with observations.

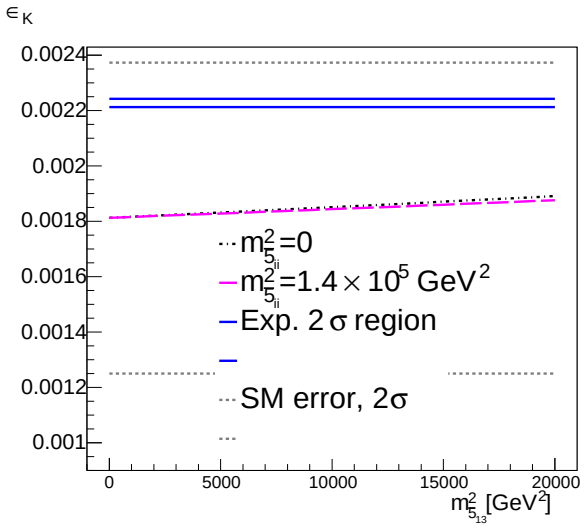

Figure 15: *The 2 σ experimental region of $|\epsilon_K|$ is $(2.213 - 2.243) \times 10^{-3}$, and the range of the supersymmetric prediction together with the 2 σ Standard Model error is $(1.25 - 2.37) \times 10^{-3}$.*

.

4.1.3 The $(2,3)$ sector

In this sector the most constraining parameter is the neutron EDM. Just as in the case of sector $(1,3)$, the neutron EDM is well below the present experimental limit and up to a value of $m^2_{\bar{5}_{23}} \approx 3.2 \times 10^3$ GeV^2 (for $m^2_{\bar{5}_{ii}} = 0$) also below the expected limit of the future sensitivity of $O(10^{-28})$ e-cm. In Fig. 16 we show the neutron EDM as a function of $m^2_{\bar{5}_{23}}$ for three values of $m^2_{\bar{5}_{ii}} = 0$, 6×10^4 GeV^2 and 1.4×10^5 GeV^2. As in Fig. 13, we show current constraints from the neutron EDM in the left panels and future limits on right. In the top row for the present experimental limit, while in the second for the future sensitivity. In the top row, $m^2_{10} = 0$ ($c = d = 0$). In the middle row, $m^2_{10_{ii}} = m^2_{5_{ii}}$ ($c = a$, $d = 0$), and in the bottom row, we plot d_n versus $d = m^2_{10_{23}}$ with $c = a$ and $b = 0$. As one can see, there are no current constraints on either b or d for our allowed range in a and c. However, we expect that future constraints can place a limit of about $b \lesssim 3500$ GeV^2 and $d \lesssim 8 \times 10^4$ GeV^2.

Other parameters that are affected by allowing for a non-zero off-diagonal parameter in the (23) sector are ϵ_K, BR$(\mu \to e\gamma)$, BR$(\tau \to \mu\gamma)$ and BR$(\tau \to e\gamma)$, which however remain within the experimental limits. Once again, for ϵ_K we also rely on taking into account the Standard Model uncertainty to obtain compatibility. We note also that BR$(B \to X_s\gamma)$ is sensitive to changes in this sector, though this is noticeable only for light ($\lesssim 1$ TeV) supersymmetric spectra [27].

Table 8 summarize the constraints on the MaxSFV scenario in the (12), (13) and (23) sectors. The numbers in the various entries of the Table are the maximum values in GeV^2 of b (in the soft supersymmetry-breaking fiveplet mass-sequared matrix) where $b/a = 1$ is allowed by present (and possible future) data, and the maximum values of b (in the soft supersymmetry-breaking tenplet mass-sequared matrix) where $d/c = 1$ is allowed by present (and possible future) data. We see that the MaxSFV scenario in the fiveplet (12) sector is consistent with the present data for $m^2_{\bar{5}} \lesssim 170$ GeV^2, increasing to $\lesssim 520$ GeV^2 in the tenplet (12) sector, $\lesssim 8000$ GeV^2 in the fiveplet (13) sector, and $\lesssim 1800$ GeV^2 in the tenplet (13) sector. There are currently no constraints on MaxSFV in the (23) sector, though this may change with future data.

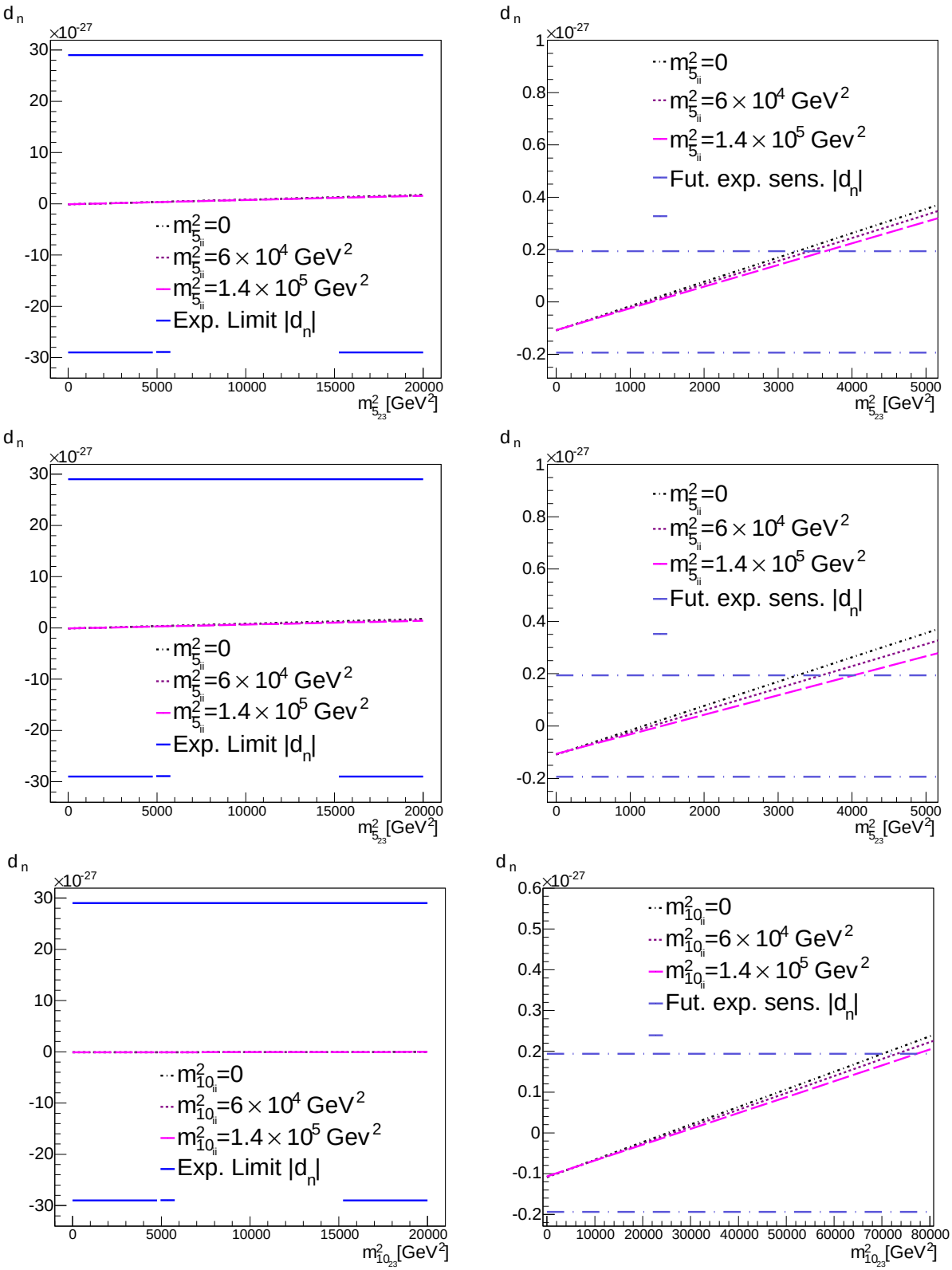

Figure 16: *Top:* $m^2_{\tilde{5}_{23}}$ *vs.* d_n *for* $m^2_{\tilde{5}_{ii}} = 0,\ 6\times10^5\ GeV^2$ *and* $1.4\times10^5\ GeV^2$. *Here* $m^2_{10_{ii}} = 0$ $(c = d = 0)$. *For definiteness, we have used the value of* 1.94×10^{-28} *[52], for the future sensitivity. Other values (all of* $O(10^{-28})$*) can be found in [41]. Middle: the same as above, except for* $m^2_{10_{ii}} = m^2_{\tilde{5}_{ii}}$ $(c = a,\ d = 0)$. *Bottom: the case for* $m^2_{10_{23}}$ *vs.* d_n *for* $m^2_{10_{ii}} = m^2_{\tilde{5}_{ii}}$ $(c = a,\ b = 0)$.

Sector	(12)	(13)	(23)
$m^2_{\bar{5}}$ - present	170	8000	-
$m^2_{\bar{5}}$ - future	-	230	3400
m^2_{10} - present	520	1800	-
m^2_{10} - future	-	1550	73000

Table 8: *Summary of constraints on $b = a$ and $d = c$ in the MaxSFV scenario. All quantities are in GeV^2.*

5 Summary

We have explored in this paper the phenomenological constraints on super-GUT models, in which soft supersymmetry breaking inputs are postulated at some scale M_{in} intermediate between $M_{\rm GUT}$ and the Planck scale, that are imposed by upper limits on flavor and CP violation. For this purpose, we have chosen a benchmark supersymmetric model (**B** in (19) above) motivated by no-scale supergravity that is consistent with other constraints from the LHC (e.g., m_h and the non-appearance of sparticles during Run 1) and cosmology (e.g., the density of cold dark matter and inflation). Within this framework we have considered four possible scenarios for Yukawa couplings that are compatible with CKM mixing and its extension to sparticles. Consideration of the runnings of model parameters in two of these scenarios (A3 and A4 in Eqs. 17 and 18 above) were found to be generally *incompatible* with the flavor-violation constraints, and not pursued further. However, the other two scenarios (A1 and A2 in Eqs. 15 and 16 above) were found to be *compatible* with the flavour-violation constraints. They have quite different predictions, and serve to illustrate the range of possibilities for future flavor-violation measurements in no-scale super-GUTs.

We then considered possible deformations of the no-scale scenario, in which the soft supersymmetry-breaking scalar masses m_0 are allowed to be non-zero but much smaller than the gaugino mass $m_{1/2}$ at M_{in}. In particular, we have investigated the maximal magnitudes of off-diagonal terms in the sfermion mass-squared matrices m_0^2 for the SU(5) fiveplets and tenplets, and the possibility that these might be as large as the diagonal entries, a scenario we call MaxSFV. We find that the off-diagonal (12) entry in the fiveplet mass-squared matrix could be as large as the diagonal entries if the latter are $\simeq 170$ GeV^2 and $\simeq 520$ GeV^2 in the $m^2_{\bar{5}}$ and m^2_{10} mass-squared matrices, respectively. The corresponding numbers in the (13) sector are $\simeq 8 \times 10^3$ GeV^2 in the fiveplet mass-squared matrix and $\simeq 1.8 \times 10^3$ GeV^2 for the tenplets. There are currently no useful bounds in the (23) sector. The future sensitivity in d_n would be sensitive to MaxSFV in the (13) sector of $\mathcal{O}(230)$ GeV^2 for the for the fiveplets and of $\mathcal{O}(1.5 \times 10^3)$ GeV^2 for the tenplets, and of $\mathcal{O}(3.4 \times 10^3)$ GeV^2 in the (23) sector for the fiveplets and $\mathcal{O}(7.3 \times 10^4)$ GeV^2 for the tenplets.

Within these limits, *there would be no supersymmetric flavour problem* associated with sfermion masses in the class of near-no-scale super-GUTs discussed in this paper.

A Three-family beta functions in SU(5)

Many of the RGEs for the single-family case can be found in [19, 53, 17, 14]. Here we list the complete set of RGEs relevant for the 3-family case. Whilst the beta function for λ' in

EQNO does not change with respect to the one-family case, that is

$$\frac{\mathrm{d}\lambda'}{\mathrm{dt}} = \frac{\lambda'}{16\pi^2}\left(\frac{63\lambda'^2}{20} + 3\lambda^2 \ - 30\mathrm{g}_5^2\right) ,$$

the other beta functions change as follows:

$$\begin{aligned}
\frac{\mathrm{d}\lambda}{\mathrm{dt}} &= \frac{\lambda}{16\pi^2}\left(48\mathrm{Tr}[\mathrm{h}_{10}^\dagger \mathrm{h}_{10}] + 2\ \mathrm{Tr}[\mathrm{h}_{\bar{5}}^\dagger \mathrm{h}_{\bar{5}}] + \frac{53\lambda^2}{5} + \frac{21\lambda'^2}{20} - \frac{98\ \mathrm{g}_5^2}{5}\right) , \\
\frac{\mathrm{dh}_{10}}{\mathrm{dt}} &= \frac{1}{16\pi^2}\Big[\ \mathrm{h}_{10}\left(48\mathrm{Tr}[\mathrm{h}_{10}^\dagger \mathrm{h}_{10}] + \frac{24\ \lambda^2}{5} - \frac{96\mathrm{g}_5^2}{5}\right) + 96\ \mathrm{h}_{10}\mathrm{h}_{10}^\dagger \mathrm{h}_{10} \\
&+ \ \mathrm{h}_{10}\mathrm{h}_{\bar{5}}^\dagger \mathrm{h}_{\bar{5}} + \mathrm{h}_{\bar{5}}\mathrm{h}_{\bar{5}}^\dagger \mathrm{h}_{10}\Big] , \\
\frac{\mathrm{dh}_{\bar{5}}}{\mathrm{dt}} &= \frac{1}{16\pi^2}\Big[\mathrm{h}_{\bar{5}}\left(2\mathrm{Tr}[\mathrm{h}_{\bar{5}}^\dagger \mathrm{h}_{\bar{5}}] + \frac{24\lambda^2}{5} - \frac{84\ \mathrm{g}_5^2}{5}\right) + 48\mathrm{h}_{\bar{5}}\mathrm{h}_{10}^\dagger \mathrm{h}_{10} \\
&+ \ 3\ \mathrm{h}_{\bar{5}}\mathrm{h}_{\bar{5}}^\dagger \mathrm{h}_{\bar{5}}\Big] ;
\end{aligned}$$

$$\begin{aligned}
\frac{\mathrm{dA}_\lambda}{\mathrm{dt}} &= \frac{1}{8\pi^2}\left[48\mathrm{Tr}[\mathrm{h}_{10}^\dagger \mathrm{a}_{10}] + 2\ \mathrm{Tr}[\mathrm{h}_{\bar{5}}^\dagger \mathrm{a}_{\bar{5}}] + \frac{53\lambda^2\mathrm{A}_\lambda}{5} + \frac{21\ \mathrm{A}_{\lambda'}\lambda'^2}{20} - \frac{98\mathrm{g}_5^2\mathrm{M}_5}{5}\right] , \\
\frac{\mathrm{dA}_{\lambda'}}{\mathrm{dt}} &= \frac{1}{8\pi^2}\left[3\lambda^2\mathrm{A}_\lambda + \frac{63\mathrm{A}_{\lambda'}\lambda'^2}{20} - 30\mathrm{g}_5^2\ \mathrm{M}_5\right] , \\
\frac{\mathrm{da}_{10}}{\mathrm{dt}} &= \frac{1}{16\pi^2}\Big[\frac{24}{5}\mathrm{a}_{10}\left(10\mathrm{Tr}[\mathrm{h}_{10}^\dagger \mathrm{h}_{10}] + \lambda^2 - 8\mathrm{g}_5^2\right) \\
&+ \ \frac{48}{5}\mathrm{h}_{10}\left(10\mathrm{Tr}[\mathrm{h}_{10}^\dagger \mathrm{a}_{10}] + |\lambda|^2\mathrm{A}_\lambda - 4\mathrm{g}_5^2\mathrm{M}_5\right) \\
&+ \ 144\ \mathrm{a}_{10}\mathrm{h}_{10}^\dagger \mathrm{h}_{10} + 144\ \mathrm{h}_{10}\mathrm{h}_{10}^\dagger \mathrm{a}_{10} \\
&+ \ \mathrm{a}_{10}\mathrm{h}_{\bar{5}}^\dagger \mathrm{h}_{\bar{5}} + \mathrm{h}_{\bar{5}}\mathrm{h}_{\bar{5}}^\dagger \mathrm{a}_{10} + 2(\mathrm{a}_{\bar{5}}\mathrm{h}_{\bar{5}}^\dagger \mathrm{h}_{10} + \mathrm{h}_{10}\mathrm{h}_{\bar{5}}^\dagger \mathrm{a}_{\bar{5}})\Big] , \qquad (30) \\
\frac{\mathrm{da}_{\bar{5}}}{\mathrm{dt}} &= \frac{1}{16\pi^2}\Big[\mathrm{h}_{\bar{5}}\left(4\mathrm{Tr}[\mathrm{h}_{\bar{5}}^\dagger \mathrm{a}_{\bar{5}}] + \frac{48\lambda^2\ \mathrm{A}_\lambda}{5} - \frac{168\mathrm{g}_5^2\mathrm{M}_5}{5}\right) \\
&+ \ \mathrm{a}_{\bar{5}}\left(2\ \mathrm{Tr}[\mathrm{h}_{\bar{5}}^\dagger \mathrm{h}_{\bar{5}}] + \frac{24|\lambda|^2}{5} - \frac{84\ \mathrm{g}_5^2}{5}\right) + 96\mathrm{h}_{\bar{5}}\mathrm{h}_{10}^\dagger \mathrm{a}_{10} \\
&+ \ 48\ \mathrm{a}_{\bar{5}}\mathrm{h}_{10}^\dagger \mathrm{h}_{10} + 6\mathrm{a}_{\bar{5}}\mathrm{h}_{\bar{5}}^\dagger \mathrm{h}_{\bar{5}}\ + 3\mathrm{h}_{\bar{5}}\mathrm{h}_{\bar{5}}^\dagger \mathrm{a}_{\bar{5}}\Big] ;
\end{aligned}$$

$$\begin{aligned}
\frac{\mathrm{dm}_{24}^2}{\mathrm{dt}} &= \frac{1}{8\pi^2}\left[\lambda^2\ \left(\mathrm{A}_\lambda^2 + \mathrm{m}_{24}^2 + \mathrm{m}_{5_H}^2 + \mathrm{m}_{\bar{5}_H}^2\right) + \frac{21}{20}\ \lambda'^2\left(\mathrm{A}_{\lambda'}^2 + 3\mathrm{m}_{24}^2\right) - 20\mathrm{g}_5^2\mathrm{M}_5^2\mathbf{1}\right] , \\
\frac{\mathrm{dm}_{5_H}^2}{\mathrm{dt}} &= \frac{1}{8\pi^2}\Big[3(16\mathrm{Tr}[\mathrm{a}_{10}^\dagger \mathrm{a}_{10}] + 32\ \mathrm{Tr}[\mathrm{h}_{10}\mathrm{m}_{10}^2\mathrm{h}_{10}^\dagger] + 16\mathrm{m}_{5_H}^2\ \mathrm{Tr}[\mathrm{h}_{10}^\dagger \mathrm{h}_{10}]) \\
&+ \ \frac{24}{5}\lambda^2\ \left(\mathrm{A}_\lambda^2 + \mathrm{m}_{24}^2 + \mathrm{m}_{5_H}^2 + \mathrm{m}_{\bar{5}_H}^2\right) - \frac{48\mathrm{g}_5^2\ \mathrm{M}_5^2}{5}\mathbf{1}\Big] , \\
\frac{\mathrm{dm}_{\bar{5}_H}^2}{\mathrm{dt}} &= \frac{1}{8\pi^2}\Big[2\ (\mathrm{Tr}[\mathrm{a}_{\bar{5}}^\dagger \mathrm{a}_{\bar{5}}] + \mathrm{Tr}[\mathrm{h}_{\bar{5}}\mathrm{m}_{10}^2\mathrm{h}_{\bar{5}}^\dagger]\ + \mathrm{Tr}[\mathrm{h}_{\bar{5}}^\dagger \mathrm{m}_{\bar{5}}^2\mathrm{h}_{\bar{5}}\mathbf{1}] \\
&+ \ \mathrm{m}_{\bar{5}_H}^2\ \mathrm{Tr}[\mathrm{h}_{\bar{5}}^\dagger \mathrm{h}_{\bar{5}}]) + \frac{24}{5}\lambda^2\ \left(\mathrm{A}_\lambda^2 + \mathrm{m}_{24}^2 + \mathrm{m}_{5_H}^2 + \mathrm{m}_{\bar{5}_H}^2\right) - \frac{48}{5}\mathrm{g}_5^2\ \mathrm{M}_5^2\mathbf{1}\Big] , \\
\frac{\mathrm{dm}_{\bar{5}}^2}{\mathrm{dt}} &= \frac{1}{16\pi^2}\Big[2(2\mathrm{a}_{\bar{5}}^\dagger \mathrm{a}_{\bar{5}} + 2\mathrm{m}_{\bar{5}_H}^2\ \mathrm{h}_{\bar{5}}^\dagger \mathrm{h}_{\bar{5}} + \mathrm{m}_{\bar{5}}^2\mathrm{h}_{\bar{5}}^\dagger \mathrm{h}_{\bar{5}} + 2\ \mathrm{h}_{\bar{5}}^\dagger \mathrm{m}_{10}^2\mathrm{h}_{\bar{5}} + \mathrm{h}_{\bar{5}}^\dagger \mathrm{h}_{\bar{5}}\mathrm{m}_{\bar{5}}^2)
\end{aligned}$$

$$
\begin{aligned}
&- \quad \frac{96\ \mathrm{g}_{\bar{5}}^2 \mathrm{M}_{\bar{5}}^2}{5}\mathbf{1}\Big] \,, \\
\frac{\mathrm{dm}_{10}^2}{\mathrm{dt}} &= \frac{1}{16\pi^2}\Big[-\frac{144}{5}\mathrm{g}_{\bar{5}}^2\mathrm{M}_{\bar{5}}^2\mathbf{1} + \mathrm{m}_{10}^2\mathrm{h}_{\bar{5}}^\dagger\mathrm{h}_{\bar{5}} + 96\ (\mathrm{m}_{5_H}^2\mathrm{h}_{10}^\dagger\mathrm{h}_{10} + \mathrm{h}_{10}^\dagger\mathrm{m}_{10}^2\mathrm{h}_{10}) \\
&+ \quad 48\ (\mathrm{m}_{10}^2\mathrm{h}_{10}^\dagger\mathrm{h}_{10} + \mathrm{h}_{10}^\dagger\mathrm{h}_{10}\mathrm{m}_{10}^2) + 2\ (48\mathrm{a}_{10}^\dagger\mathrm{a}_{10} + \mathrm{a}_{\bar{5}}^\dagger\mathrm{a}_{\bar{5}} + \mathrm{m}_{\bar{5}_H}^2\ \mathrm{h}_{\bar{5}}^\dagger\mathrm{h}_{\bar{5}} + \mathrm{h}_{\bar{5}}^\dagger\mathrm{m}_{\bar{5}}^2\mathrm{h}_{\bar{5}}) \\
&+ \quad \mathrm{h}_{\bar{5}}^\dagger\mathrm{h}_{\bar{5}}\ \mathrm{m}_{10}^2\Big]\ ; \qquad (31)
\end{aligned}
$$

$$
\begin{aligned}
\frac{\mathrm{dB}_{24}}{\mathrm{dt}} &= \frac{1}{8\pi^2}\left[2\lambda^2\mathrm{A}_\lambda + \frac{21\mathrm{A}_{\lambda'}\lambda'^2}{10} - 20\mathrm{g}_{\bar{5}}^2\mathrm{M}_5\mathbf{1}\right] , \\
\frac{\mathrm{dB}_5}{\mathrm{dt}} &= \frac{1}{8\pi^2}\left[48\mathrm{Tr}[\mathrm{h}_{10}^\dagger\mathrm{a}_{10}] + 2\ \mathrm{Tr}[\mathrm{h}_{\bar{5}}^\dagger\mathrm{a}_{\bar{5}}] + \frac{48\lambda^2\mathrm{A}_\lambda}{5} - \frac{48\ \mathrm{g}_{\bar{5}}^2\mathrm{M}_5}{5}\mathbf{1}\right] . \qquad (32)
\end{aligned}
$$

B Transformation rules

The physical mass eigenstates for each flavor are calculated in the SCKM basis by diagonalizing the 6×6 matrices

$$
\begin{aligned}
(\mathcal{M}_f^{\mathrm{SCKM}})_{ij}^2 &= \begin{bmatrix} \hat{m}_{fLL}^2 & \hat{m}_{fLR}^2 \\ \hat{m}_{fLR}^2 & \hat{m}_{fRR}^2 \end{bmatrix}_{ij} \equiv (\widehat{\mathcal{M}}_f^2)_{ij} \\
&= \begin{bmatrix} \left(V_L^{f\dagger} m_Q^2 V_L^f\right)_{ij} + (\hat{m}_{f_i})^2\delta_{ij} + D_L^f & -((V_L^{f\dagger} a_f V_R^f)_{ij} v_f + \mu^* \tan^p\beta\ \hat{m}_{f_i}\delta_{ij}) \\ -((V_L^f a_f^\dagger V_R^{f\dagger})_{ij} v_f + \mu \tan^p\beta\ \hat{m}_{f_i}\delta_{ij}) & (V_R^{f\dagger} m_{f_R}^2 V_R^f)_{ij} + (\hat{m}_{f_i})^2\delta_{ij} + D_R^f \end{bmatrix}, \\
p &= \begin{cases} 1, & f = D, L \\ -1, & f = U. \end{cases} , \qquad (33)
\end{aligned}
$$

where $\hat{m}_f$ are the diagonal quark mass matrices. We use the following notation for the matrices diagonalizing the soft mass-squared matrices:

$$
K\ (\mathcal{M}_f^{\mathrm{SCKM}})^2\ K^\dagger = \mathrm{diag}(\mathrm{m}_{\tilde{\ell}_1}^2, \ldots, \mathrm{m}_{\tilde{\ell}_6}^2), \qquad (34)
$$

where $m_{\tilde{\ell}_i}^2$ are the mass eigenstates.

To help understand the impact of the RGEs on the final parameter values at M_{EW}, we show contributions to the beta functions in the SCKM basis taken from Eq. (4.34) of [54]:

$$
\begin{aligned}
\beta_{m_D^2}^{(1)} &\supset m_D^2 h_D h_D^\dagger, \quad h_D m_Q^2 h_D^\dagger, \quad h_D h_D^\dagger m_D^2, \quad m^2 h_D h_D^\dagger, \\
\beta_{m_Q^2}^{(1)} &\supset m_Q^2 h_U^\dagger h_U, \quad m_Q^2 h_D^\dagger h_D, \quad h_U^\dagger h_U m_Q^2, \quad h_D^\dagger h_D m_Q^2, \quad h_U^\dagger m_U^2 h_U, \quad h_D^\dagger m_D^2 h_D, \\
&\quad a_D^\dagger a_D, \quad m^2 h_U^\dagger h_U, \quad m^2 h_D^\dagger h_D, \qquad (35)
\end{aligned}
$$

where m^2 is a mass-squared term and not a matrix, for example $m^2 = m_{H_d}^2$. Using $dm^2 = \int dt \beta_{m^2}^{(1)}/16\pi^2$, we can calculate the form of the mass-squared terms at the EW scale in the SCKM basis. In addition to the transformation given in Eq. (20), the general transformations for all the terms appearing in Eq (35), independent of the Ansatz, are as follows:

Transformation of terms in m_Q^2 *Transformation of terms in* m_D^2 :

to the SCKM basis :

1. $m_Q^2 h_D^\dagger h_D \to \hat{m}_Q^2 \hat{h}_D^2$
2. $m_Q^2 h_U^\dagger h_U \to \hat{m}_Q^2 V_{\rm CKM}^\dagger \hat{h}_U^2 V_{\rm CKM}$
3. $h_U^\dagger h_U m_Q^2 \to V_{\rm CKM}^\dagger \hat{h}_U^2 V_{\rm CKM} \hat{m}_Q^2$
4. $h_D^\dagger h_D m_Q^2 \to \hat{h}_D^2 \hat{m}_Q^2$
5. $h_U^\dagger m_U^2 h_U \to {V_{\rm CKM}}^\dagger \hat{h}_U \left(V_R^{u\dagger} m_U^2 V_R^U \right) \hat{h}_U V_{\rm CKM}$
6. $h_D^\dagger m_D^2 h_D \to \hat{h}_D^\dagger \hat{m}_D^2 \hat{h}_D$
7. $a_D^\dagger a_D \to \hat{a}_D^\dagger \hat{a}_D$
8. $m^2 h_U^\dagger h_U \to m^2 V_{\rm CKM}^\dagger \hat{h}_U V_{\rm CKM}$
9. $m^2 h_D^\dagger h_D \to \hat{h}_D^\dagger \hat{h}_D$.

1. $m_D^2 h_D h_D^\dagger \to V_R^{d\dagger} m_D^2 V_R^D \hat{h}_D^2$
2. $h_D m_Q^2 h_D^\dagger \to \hat{h}_D \hat{m}_Q^2 \hat{h}_D$
3. $h_D h_D^\dagger m_D^2 \to \hat{h}_D \left(V_{DR}^\dagger m_D^2 V_{DR} \right)$
4. $m^2 h_D h_D^\dagger \to m^2 \hat{h}_D \hat{h}_D^\dagger$

(36)

The transformations (36) to the SCKM basis are valid at all energy scales. With the exception of the fifth entry in (36) for the transformations of m_Q^2, the rest of the terms have the same form. (Actually, the initial value of $\hat{m}_Q^2 = V_L^{D\dagger} m_Q^2 V_L^D$ also has the same form, since $V_L^D = V_{\rm CKM}$ for both cases.) The fifth entry in (36) for the transformation of m_Q^2, could potentially be different, because it is not given only in terms of $V_{\rm CKM}$ or squared quark masses, but V_R^U. However, since in both Ansätze we have the same form of V_R^U and m_U^2, i.e., diagonal matrices, this term would not make a numerical difference in either Ansatz. Hence the only differences in $\hat{m}_Q^2$ at $M_{\rm GUT}$ are the different values of the off-diagonal elements in m_Q^2 and m_D^2. There are more differences in the transformations of terms in $\hat{m}_D^2$, since terms (1) and (3) of (36) explicitly involve V_R^D, which is different in the two cases.

Transformation of terms in a_D

1. $a_D h_D^\dagger h_D \to \hat{a}_D \hat{h}_D^2 = V_L^{D\dagger} a_D V_R^D \hat{h}_D^2$
2. $a_D h_U^\dagger h_U \to \hat{a}_D \hat{h}_U^2 V_R^{U\dagger} V_R^D = V_L^{D\dagger} a_D V_R^D \hat{h}_U^2 V_R^{U\dagger} V_R^D$
3. $h_D h_U^\dagger a_D \to \hat{h}_D^2 \hat{a}_D = \hat{h}_D^2 V_L^{D\dagger} a_D V_R^D$
4. $h_D h_U^\dagger a_U \to \hat{h}_D \left(V_R^{D\dagger} V_R^U \hat{h}_U V_L^{U\dagger} a_U V_R^D \right)$.

(37)

Acknowledgements

The work of JE was supported in part by the London Centre for Terauniverse Studies (LCTS), using funding from the European Research Council via the Advanced Investigator Grant 26732, and in part by the STFC Grant ST/L000326/1. The work of K.A.O. was supported in part by DOE grant de-sc0011842 at the University of Minnesota. We thank J. Rosiek for help with `SUSY_FLAVOR`.

References

[1] J. R. Ellis and D. V. Nanopoulos, Phys. Lett. B **110** (1982) 44.

[2] R. Barbieri and R. Gatto, Phys. Lett. B **110** (1982) 211.

[3] Z. Chacko, M. A. Luty, A. E. Nelson and E. Ponton, JHEP **0001**, 003 (2000) [hep-ph/9911323]; M. Schmaltz and W. Skiba, Phys. Rev. D **62**, 095005 (2000) [arXiv:hep-ph/0001172]; M. Schmaltz and W. Skiba, Phys. Rev. D **62**, 095004 (2000) [arXiv:hep-ph/0004210].

[4] S. Dimopoulos and H. Georgi, Nucl. Phys. B **193** (1981) 150. doi:10.1016/0550-3213(81)90522-8

[5] N. Sakai, Z. Phys. C **11** (1981) 153. doi:10.1007/BF01573998

[6] M. Drees and M. M. Nojiri, Phys. Rev. D **47** (1993) 376 [arXiv:hep-ph/9207234]; G. L. Kane, C. F. Kolda, L. Roszkowski and J. D. Wells, Phys. Rev. D **49** (1994) 6173 [arXiv:hep-ph/9312272]; H. Baer and M. Brhlik, Phys. Rev. D **53** (1996) 597 [arXiv:hep-ph/9508321]; Phys. Rev. D **57** (1998) 567 [arXiv:hep-ph/9706509]; J. R. Ellis, T. Falk, K. A. Olive and M. Schmitt, Phys. Lett. B **388** (1996) 97 [arXiv:hep-ph/9607292]; Phys. Lett. B **413** (1997) 355 [arXiv:hep-ph/9705444]; J. R. Ellis, T. Falk, G. Ganis, K. A. Olive and M. Schmitt, Phys. Rev. D **58** (1998) 095002 [arXiv:hep-ph/9801445]; V. D. Barger and C. Kao, Phys. Rev. D **57** (1998) 3131 [arXiv:hep-ph/9704403]; J. R. Ellis, T. Falk, G. Ganis and K. A. Olive, Phys. Rev. D **62** (2000) 075010 [arXiv:hep-ph/0004169]; H. Baer, M. Brhlik, M. A. Diaz, J. Ferrandis, P. Mercadante, P. Quintana and X. Tata, Phys. Rev. D **63** (2001) 015007 [arXiv:hep-ph/0005027]; J. R. Ellis, T. Falk, G. Ganis, K. A. Olive and M. Srednicki, Phys. Lett. B **510** (2001) 236 [arXiv:hep-ph/0102098]; V. D. Barger and C. Kao, Phys. Lett. B **518** (2001) 117 [arXiv:hep-ph/0106189]; L. Roszkowski, R. Ruiz de Austri and T. Nihei, JHEP **0108** (2001) 024 [arXiv:hep-ph/0106334]; A. Djouadi, M. Drees and J. L. Kneur, JHEP **0108** (2001) 055 [arXiv:hep-ph/0107316]; U. Chattopadhyay, A. Corsetti and P. Nath, Phys. Rev. D **66** (2002) 035003 [arXiv:hep-ph/0201001]; J. R. Ellis, K. A. Olive and Y. Santoso, New Jour. Phys. **4** (2002) 32 [arXiv:hep-ph/0202110]; H. Baer, C. Balazs, A. Belyaev, J. K. Mizukoshi, X. Tata and Y. Wang, JHEP **0207** (2002) 050 [arXiv:hep-ph/0205325]; R. Arnowitt and B. Dutta, arXiv:hep-ph/0211417.

[7] R. Barbieri, S. Ferrara and C. A. Savoy, Phys. Lett. B **119**, 343 (1982).

[8] M. Dine, A. E. Nelson and Y. Shirman, Phys. Rev. D **51**, 1362 (1995) [hep-ph/9408384].

[9] S. A. R. Ellis and G. L. Kane, arXiv:1505.04191 [hep-ph].

[10] M. Ciuchini, A. Masiero, P. Paradisi, L. Silvestrini, S. K. Vempati and O. Vives, Nucl. Phys. B **783**, 112 (2007) doi:10.1016/j.nuclphysb.2007.05.032 [hep-ph/0702144 [HEP-PH]].

[11] E. Cremmer, S. Ferrara, C. Kounnas and D. V. Nanopoulos, Phys. Lett. B **133**, 61 (1983); J. R. Ellis, C. Kounnas and D. V. Nanopoulos, Nucl. Phys. B **247**, 373 (1984).

[12] G. F. Giudice, R. Rattazzi, Phys. Rept. **322** (1999) 419-499. [hep-ph/9801271].

[13] J. R. Ellis, D. V. Nanopoulos and K. A. Olive, Phys. Lett. B **525** (2002) 308 [hep-ph/0109288].

[14] J. Ellis, A. Mustafayev and K. A. Olive, Eur. Phys. J. C **69**, 219 (2010) [arXiv:1004.5399 [hep-ph]].

[15] J. Ellis, D. V. Nanopoulos and K. A. Olive, Phys. Rev. D **89** (2014) 043502 [arXiv:1310.4770 [hep-ph]].

[16] L. Calibbi, Y. Mambrini and S. K. Vempati, JHEP **0709**, 081 (2007) [arXiv:0704.3518 [hep-ph]]; L. Calibbi, A. Faccia, A. Masiero and S. K. Vempati, Phys. Rev. D **74**, 116002 (2006) [arXiv:hep-ph/0605139]; E. Carquin, J. Ellis, M. E. Gomez, S. Lola and J. Rodriguez-Quintero, JHEP **0905** (2009) 026 [arXiv:0812.4243 [hep-ph]]; J. Ellis, A. Mustafayev and K. A. Olive, Eur. Phys. J. C **71**, 1689 (2011) [arXiv:1103.5140 [hep-ph]].

[17] J. Ellis, A. Mustafayev and K. A. Olive, Eur. Phys. J. C **69**, 201 (2010) [arXiv:1003.3677 [hep-ph]].

[18] E. Dudas, Y. Mambrini, A. Mustafayev and K. A. Olive, Eur. Phys. J. C **72**, 2138 (2012) [Erratum-ibid. C **73**, 2430 (2013)] [arXiv:1205.5988 [hep-ph]].

[19] N. Polonsky and A. Pomarol, Phys. Rev. Lett. **73**, 2292 (1994) [arXiv:hep-ph/9406224], and Phys. Rev. D **51** (1995) 6532 [arXiv:hep-ph/9410231].

[20] J. R. Ellis, K. A. Olive, Y. Santoso and V. C. Spanos, Phys. Lett. B **573**, 162 (2003) [hep-ph/0305212].

[21] F. Borzumati and T. Yamashita, Prog. Theor. Phys. **124**, 761 (2010) [arXiv:0903.2793 [hep-ph]].

[22] J. R. Ellis and M. K. Gaillard, Phys. Lett. B **88** (1979) 315. doi:10.1016/0370-2693(79)90476-3

[23] K. A. Olive *et al.* [Particle Data Group Collaboration], Chin. Phys. C **38**, 090001 (2014).

[24] K. G. Chetyrkin, J. H. Kuhn and M. Steinhauser, Comput. Phys. Commun. **133**, 43 (2000) [hep-ph/0004189].

[25] Z. -z. Xing, H. Zhang and S. Zhou, Phys. Rev. D **77**, 113016 (2008) [arXiv:0712.1419 [hep-ph]].

[26] Information about this code is available from K. A. Olive: it contains important contributions from T. Falk, G. Ganis, A. Mustafayev, J. McDonald, F. Luo, K. A. Olive, P. Sandick, Y. Santoso, V. Spanos, and M. Srednicki.

[27] K. A. Olive and L. Velasco-Sevilla, JHEP **0805**, 052 (2008) [arXiv:0801.0428 [hep-ph]].

[28] G. Aad *et al.* [ATLAS Collaboration], JHEP **1409** (2014) 176 [arXiv:1405.7875 [hep-ex]]; JHEP **1510**, 054 (2015) doi:10.1007/JHEP10(2015)054 [arXiv:1507.05525 [hep-ex]]; JHEP **1406** (2014) 055 [arXiv:1402.4770 [hep-ex]].

[29] P. A. R. Ade *et al.* [Planck Collaboration], arXiv:1502.01589 [astro-ph.CO].

[30] S. Heinemeyer, W. Hollik and G. Weiglein, Eur. Phys. J. C **9** (1999) 343 [arXiv:hep-ph/9812472]; S. Heinemeyer, W. Hollik and G. Weiglein, Comput. Phys. Commun. **124** (2000) 76 [arXiv:hep-ph/9812320]; M. Frank *et al.*, JHEP **0702** (2007) 047 [arXiv:hep-ph/0611326]; T. Hahn, S. Heinemeyer, W. Hollik, H. Rzehak and G. Weiglein, Comput. Phys. Commun. **180** (2009) 1426. see `http://www.feynhiggs.de`.

[31] G. Aad *et al.* [ATLAS and CMS Collaborations], Phys. Rev. Lett. **114** (2015) 191803 doi:10.1103/PhysRevLett.114.191803 [arXiv:1503.07589 [hep-ex]].

[32] K. De Bruyn, R. Fleischer, R. Knegjens, P. Koppenburg, M. Merk and N. Tuning, Phys. Rev. D **86**, 014027 (2012) doi:10.1103/PhysRevD.86.014027 [arXiv:1204.1735 [hep-ph]].

[33] A. Arbey, M. Battaglia, F. Mahmoudi and D. Martnez Santos, Phys. Rev. D **87**, 035026 (2013) doi:10.1103/PhysRevD.87.035026 [arXiv:1212.4887 [hep-ph]].

[34] J. Rosiek, Comput. Phys. Commun. **188**, 208 (2014) [arXiv:1410.0606 [hep-ph]]; A. Crivellin, J. Rosiek, P. H. Chankowski, A. Dedes, S. Jaeger and P. Tanedo, Comput. Phys. Commun. **184**, 1004 (2013) [arXiv:1203.5023 [hep-ph]]; J. Rosiek, P. Chankowski, A. Dedes, S. Jager and P. Tanedo, Comput. Phys. Commun. **181**, 2180 (2010) [arXiv:1003.4260 [hep-ph]].

[35] R.Aaij *et al.* [LHCb and CMS Collaborations], LHCb-CONF-2013-012, CMS PAS BPH-13-007; V. Khachatryan *et al.* [CMS and LHCb Collaborations], Nature **522**, 68 (2015) [arXiv:1411.4413 [hep-ex]].

[36] S. Jäger, Eur. Phys. J. C **59**, 497 (2009) [arXiv:0808.2044 [hep-ph]].

[37] W. Altmannshofer, A. J. Buras, S. Gori, P. Paradisi and D. M. Straub, Nucl. Phys. B **830** (2010) 17 [arXiv:0909.1333 [hep-ph]].

[38] M. Arana-Catania, S. Heinemeyer, and M. Herrero, *Phys.Rev.* **D88** (2013) 015026, [arXiv:1304.2783].

[39] S. AbdusSalam and L. Velasco-Sevilla. In preparation. Bounds extracted from a comprehensive scan are compatible with the conditions presented here.

[40] M. Pospelov and A. Ritz, Annals Phys. **318**, 119 (2005) doi:10.1016/j.aop.2005.04.002 [hep-ph/0504231].

[41] J. L. Hewett *et al.*, doi:10.2172/1042577 arXiv:1205.2671 [hep-ex].

[42] T. Aoyama, M. Hayakawa, T. Kinoshita and M. Nio, Phys. Rev. Lett. **109**, 111807 (2012) [arXiv:1205.5368 [hep-ph]].

[43] J. Adam *et al.* [MEG Collaboration], Phys. Rev. Lett. **110**, 201801 (2013) doi:10.1103/PhysRevLett.110.201801 [arXiv:1303.0754 [hep-ex]].

[44] BaBar Collaboration, B. Aubert *et al.*, *Phys.Rev.Lett.* **104** (2010) 021802, [arXiv:0908.238]

[45] Heavy Flavor Averaging Group, Y. Amhis *et al.*, arXiv:1207.1158 [hep-ex].

[46] E. Gabrielli, A. Masiero and L. Silvestrini, Phys. Lett. B **374**, 80 (1996) doi:10.1016/0370-2693(96)00158-X [hep-ph/9509379].

[47] J. Kersten and L. Velasco-Sevilla, Eur. Phys. J. C **73**, no. 4, 2405 (2013) doi:10.1140/epjc/s10052-013-2405-y [arXiv:1207.3016 [hep-ph]].

[48] J. Brod and M. Gorbahn, Phys. Rev. Lett. **108**, 121801 (2012) doi:10.1103/PhysRevLett.108.121801 [arXiv:1108.2036 [hep-ph]].

[49] J. Kersten, J. h. Park, D. Stöckinger and L. Velasco-Sevilla, JHEP **1408**, 118 (2014) doi:10.1007/JHEP08(2014)118 [arXiv:1405.2972 [hep-ph]].

[50] P. Mertens and C. Smith, JHEP **1108**, 069 (2011) doi:10.1007/JHEP08(2011)069 [arXiv:1103.5992 [hep-ph]].

[51] A. Dedes, J. Rosiek and P. Tanedo, Phys. Rev. D **79**, 055006 (2009) doi:10.1103/PhysRevD.79.055006 [arXiv:0812.4320 [hep-ph]].

[52] I. Altarev *et al.*, Nucl. Instrum. Meth. A **611**, 133 (2009). doi:10.1016/j.nima.2009.07.046.

[53] H. Baer, M. A. Diaz, P. Quintana and X. Tata, JHEP **0004**, 016 (2000) [arXiv:hep-ph/0002245].

[54] S. P. Martin and M. T. Vaughn, Phys. Rev. D **50**, 2282 (1994) [Erratum-ibid. D **78**, 039903 (2008)] [hep-ph/9311340].